Boundary Layer Structure and Dynamics in Outer Hurricane Rainbands. Part I: Mesoscale Rainfall and Kinematic Structure

MARK D. POWELL

NOAA Hurricane Research Division, AOML, Miami, Florida

(Manuscript received 21 March 1989, in final form 9 November 1989)

ABSTRACT

Results of hurricane boundary layer experiments conducted in outer rainbands of Hurricanes Josephine (1984) and Earl (1986) are presented. Comparisons of precipitation and kinematic structures in these storms and in Hurricane Floyd (1981) indicate that principal rainbands have common characteristic mesoscale and convective-scale features in the boundary layer. The two-dimensional mesoscale structure suggests that these rainbands are made up of a linear aggregate of cellular reflectivity elements (on the inner, upshear side of the band) and stratiform rain (on the outer downshear side). The bands are oriented perpendicular to the shear above the boundary layer and cells move downband at about 85% of the density-weighted mean wind speed of the 0.2–6 km layer. The boundary-layer wind field is strongly influenced by the rainband with alongband and crossband wind maxima located on the outer side of the band axis, and minima 4–8 km to the inner side. Maximum crossband convergence and cyclonic shear vorticity are also found to the inner side of the rainband axis. Updrafts and downdrafts are preferentially located on the inner side of the band axis, with some downdrafts spreading out at the surface. The band-relative positions of the updraft and perturbation pressure minimum suggest that the minimum may be produced by interaction of the wind shear and the updraft. Outer hurricane rainbands show many similarities to tropical squall lines, major differences are associated with propagation and the structure of the leading and trailing edges.

1. Introduction

a. Background and objectives

The hurricane planetary boundary layer (HPBL) is of major importance in the development and maintenance of the storm. The frictional coupling of the hurricane vortex to its underlying surface produces shear- and buoyancy-induced turbulence that supplies moisture and heat to the storm and provides a sink of momentum, resulting in inflow and upward motion due to convergence. The HPBL is defined by nearly continuous turbulence that is initially produced by shear at the underlying surface. It is bounded above by the area where convective turbulence becomes important, i.e., the cloud base or a region where surface-induced turbulence no longer exists, such as an inversion.

In addition to its importance as an energy source, the HPBL has impact on the life forms within it, through destructive storm surge, wind gusts, and severe weather episodes. There is little information on the three-dimensional structure of the HPBL. Research aircraft measurements have been possible only at flight levels, which are usually above 1500 m and rarely as low as 500 m. Therefore, there is frequently only one level of data in the HPBL, except for occasional multiple-level HPBL experiments (e.g., Moss and Merceret 1976; Moss 1978), rainband experiments by Barnes et al. (1983, hereafter referred to as BZJM) and Barnes and Stossmeister (1986); and a rainband–HPBL investigation by Powell and Black (1984).

The objective of this study is to improve our knowledge of the structure of the HPBL and its interaction with rainband convection to determine: 1) a conceptual model of the three-dimensional wind, temperature and humidity structure of the HPBL in the vicinity of well-organized, convective rainbands; 2) mesoscale- and convective-scale influences, which can act to modify the HPBL structure, thereby affecting turbulent fluxes of heat, moisture and momentum at the surface and above; 3) the extent to which HPBL modification affects the coupling of the subcloud region with the convective regime above; and 4) the role of the boundary layer in the dynamics of the storm, including its importance in the development and maintenance of rainbands and storm intensification.

b. Historical development

Observational details of the structure of rainbands began to emerge upon the advent of radar as a peacetime tool for weather detection. These studies include land-based radar and surface data analyses by Wexler

Corresponding author address: Mark D. Powell, NOAA/Environmental Research Laboratories, Hurricane Research Division/AOML, 4301 Rickenbacker Causeway, Miami, FL 33149.

(1947), Ligda (1955), Ushijima (1958), Senn and Hiser (1959), Atlas et al. (1963), Tatehira (1961), Staff Members, Tokyo University (1969), and others. Much was learned about rainband reflectivity structure, cell motion and the relationship of various surface meteorological quantities. At this point it is helpful to introduce (Fig. 1) the rainband relative geometry and terminology that will be used throughout the paper. Kurihara and Tuleya (1974) and Anthes (1982) constructed conceptual models based upon past observational studies and their own numerical model results, which identified tropical cyclone rainbands as internal gravity waves. A typical conceptual model (based on these studies) shows a pressure minimum on the leading edge of the band (the outer edge farthest from the center of the storm) associated with a backing of the wind (for more crossband flow toward the band axis), a veering of the wind after the axis passes, and finally a backing of the wind to its original direction.

Early aircraft experiments in rainbands were described by Simpson and Starrett (1955) and Gentry (1964). The early aircraft investigations were penetrations of bands at only one level, above the HPBL, and suffered from lack of good quality radar and humidity measurements. Despite these drawbacks, there were some similarities between the flight-level studies and those done at the surface. Of a total of 42 aircraft band penetrations reported in the individual studies by Simpson and Gentry, 14 showed a pressure minimum on the outside edge of the band, 7 showed a minimum on the inside edge, and 21 were inconclusive. Jorgensen (1984a) compared the eyewall to outer rainbands in Hurricanes Anita (1977), Frederic (1979) and Allen (1980). He found weak band influences in the wind and thermodynamic fields of the outer rainbands that were similar in phase to eyewall fields, but were inconsistent from pass to pass.

Willoughby et al. (1982) identified symmetric rainband structures as concentric eyewalls and Willoughby et al. (1984) defined asymmetric hurricane rainband structures in the context of a quasi-stationary principal outer band, which acts as an asymptote, separating the flow within the storm core from the outside environment. Numerical experiments on the effect of a translating vortex in an environmental flow by Shapiro (1983) and Ooyama (personal communication 1986) indicate that the location of storm-stationary rainbands in asymmetric configurations about the storm center may be related to a preferential location for boundary layer convergence that is produced by an interaction of vortex motion, environmental flow, and the resultant distribution of surface friction.

Results of an HPBL experiment conducted in Hurricane Debby (1982) (Powell and Black 1984) indicated that the convective influence of a principal rainband may become more prominent at the downband or downwind end, where it could act as a barrier to the inflow of high θ_e air from outer radii. This devel-

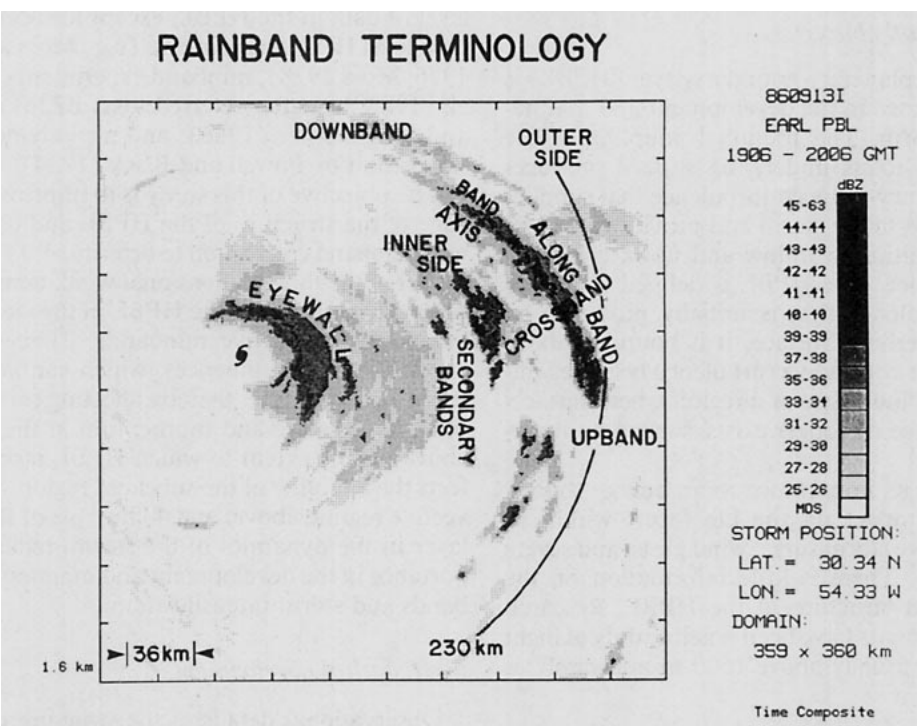

FIG. 1. Rainband terminology in the context of the Stationary Band Complex. The band crossing angle is the angle between the 230 km circle and the rainband. The band axis is the midpoint of the 25 dBZ reflectivity shading.

opment is reflected in the results obtained by BZJM from Hurricane Floyd (1981) data, but they found the barrier was only prominent in the convective portions of the band. The barrier effect may be important in controlling the inflow of unstable air and forcing the innercore and eyewall regions of the storm to use recycled, more stable air to support convection.

Ishihara et al. (1986) studied an outer stratiform typhoon rainband that contained convective cells. They collected dual-Doppler observations, from land-based radars, that suggested that not all rainbands are maintained by frictional inflow from the outer side. The typhoon band was maintained by inflow from the inner side near and above cloud base and inflow from the outer side of the band below cloud base, which formed a maximum convergence zone and mesoscale updraft on the inner side of the rainband.

Organized rainband convection occurs frequently in tropical regions and has many characteristics in common with hurricanes. The radar depiction of tropical squall lines as observed during GATE (e.g., Houze 1977) typically shows the leading edge made up of cellular reflectivity elements followed by an extensive stratiform anvil–rain region. Similar cellular and stratiform reflectivity structures are seen in hurricane rainbands, which are either storm-stationary or spirally propagating at much lower speeds than squall lines. GATE tropical squall line studies (and many other tropical and midlatitude squall line cases, e.g., Rotunno et al. 1988) usually indicate an updraft lifting over a density current or gust front downdraft at the leading edge, followed by an extensive trailing wake region topped by a mesoscale downdraft.

An important result of GATE was the discovery that these rainbands contained convective and mesoscale downdrafts that were capable of producing large wake areas of modified air that would take hours to recover to an undisturbed state. In their analysis of the Hurricane Floyd rainband, BZJM found evidence of modified air and speculated whether such areas in the vicinity of hurricane rainbands might effect eyewall convection.

In this paper and its companion, Powell (1990), I present the results of two detailed boundary layer experiments conducted in well-organized outer convective rainbands in Hurricanes Josephine (1984) and Earl (1986). Based upon these results, those from Debby (1982) (described in Powell and Black 1984), and with comparisons to Floyd (1981) and Irene (1981) (as covered by BZJM and Barnes and Stossmeister 1986, respectively), this paper contends that: 1) the similarities of principal rainband reflectivity features in several storms indicate that hurricane rainbands have distinct mesoscale and convective-scale kinematic and thermodynamic structures and governing dynamics, 2) regions of downdraft-modified boundary layer air may also be a common feature of convective hurricane rainbands, and 3) the rainbands may have additional features in common with tropical rainbands and squall lines.

2. Instrumentation, sampling, and study areas

a. Aircraft instrumentation

The NOAA aircraft in situ and remote sensing instrumentation, accuracy, and problems are described by Merceret and Davis (1981), Merceret (1983), and Powell (1988). The heart of the aircraft data system is the inertial navigation equipment (INE), which provides the attitude, position, and acceleration information necessary for navigating the aircraft and deriving the wind velocity.

The rainband precipitation structure was observed by lower fuselage (LF) and tail-mounted radars. The characteristics of these radars were summarized by Jorgensen (1984a). Aircraft size and weight limitations require small radar antennas with relatively large beam widths, which can suffer from attenuation and incomplete beam filling effects, as described by Marks (1985). The LF is a C-band (5.5 cm) radar with an antenna that rotates about a vertical axis and is most useful in conducting horizontal plan view analyses of precipitation structure. The tail radar is an X-band (3.2 cm) with an antenna that rotates about a horizontal axis. The narrow (2°) vertical beam and mode of rotation make the TA radar most useful for studying vertical cross sections and high resolution plan views of precipitation intensity for cell tracking. Due to attenuation and lack of beam filling, the maximum useful range of these radars is 60–90 km, but compositing techniques (Marks 1985) allow analysis of larger regions.

The NOAA airborne Doppler radar, (details given by see Jorgensen et al. 1983), was first used for hurricane studies in 1982 (Marks and Houze 1984). Although full analysis of the rainband wind field is in progress, small analysis regions (20 km × 20 km) using data collected over a 10 min period were available to determine wind velocity hodographs within the rainbands. The Doppler radial velocity is also examined in vertical incidence (VI) to determine vertical-motion cross sections through convection along the flight track and in an individual sweep mode to study high-resolution features of the inflow layer and convective features.

Sources of error include improper unfolding during editing of the data, high noise levels in regions of intense reflectivity gradients (usually on the edges of the detectable precipitation), lack of stationarity caused by continued evolution of the wind field during the time it takes to complete data collection for an analysis region, slight misalignments in antenna positioning, and side-lobe contamination near the sea surface. Despite these problems, area mean Doppler-derived wind velocities are consistently within 2 m s^{-1} (Powell and Black 1984) of mean aircraft winds bordering the analysis region at the same level.

b. Sampling strategy and flight patterns

High-resolution HPBL measurements in hurricanes are scarce primarily because of the difficulty of safely executing low-level flight legs in high wind shear and heavy rain conditions. To achieve the required sampling at low levels, three aircraft flight patterns were designed:

1) Stepped descents (Fig. 2a) were flown parallel to the rainband and were comprised of 1 min (downwind) or 1.5 min (upwind) sections of level flight separated by descent intervals. This pattern commenced with Omega dropwindsonde (ODW) launches at the 1500 m level and included air-expendable bathythermograph (AXBT) drops from 500 m.

2) Crossband profiles (Fig. 2b) determined HPBL profiles within, and immediately adjacent to, the rainband. When possible, these patterns were adjusted by on-board scientists to maintain sampling of a particular cellular precipitation element identified by the radar system display. In the two-aircraft HPBL experiment conducted in Hurricane Earl, to account for alongband or cellular variability (three dimensionality) of the band, pilots executed the pattern simultaneously at a 70 km separation along the rainband. At the completion of the lowest levels of the profile patterns, a fixed-bank climb was made to collect a thermodynamic sounding from the lowest level up to 1500 m.

3) Doppler patterns (Fig. 2c) acquired wind data through use of the pseudo-dual-Doppler technique, which requires two orthogonal flight legs, during which stationarity is assumed. To maximize the resolution of the airborne Doppler radar, short (~25 km) L-shaped patterns were flown with outside turns at the corner of each L. Analysis of data collected in the L pattern is part of an ongoing study and only a portion of the data (hodographs and vertical incidence cross sections) are presented here.

c. Synoptic situations and experiment chronology

Hurricane Josephine formed from a frontal trough disturbance just east of the Bahama Islands on 10 Oc-

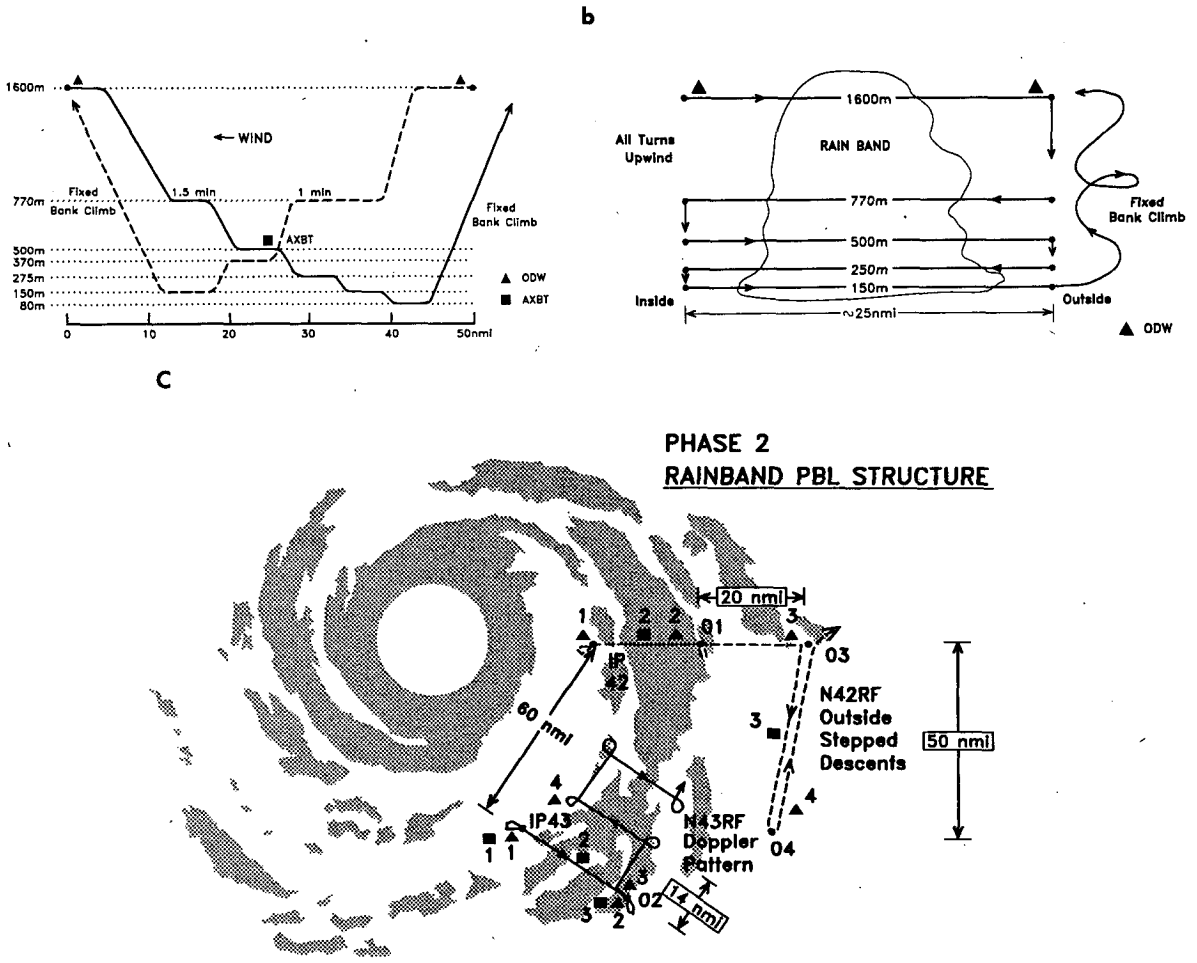

FIG. 2. Aircraft flight patterns: (a) Stepped-descent profile pattern. (b) Crossband profile pattern. (c) Airborne Doppler radar pattern and relative position of the outer stepped descents.

tober 1984. At the time of the HPBL experiment (~1030–1230 UTC) Josephine was moving north-northeast at 7 m s^{-1} and was 600 km east of the Florida–Georgia border. Maximum flight-level winds were 50 m s^{-1}. A minimum sea-level central pressure of 970 mb was estimated from flight level. The HPBL experiment consisted of an ocean response portion (see Black et al. 1988) and the rainband portion. Josephine was in a region of cool sea-surface temperatures (23°–24.5°C) associated with an oceanic front and enhanced mixing in the strong winds. The study rainband was concentric to the eye (0° band crossing angle) at 225 km northeast of the storm center (Fig. 3, arrows). Four crossband profiles and two stepped descents were executed.

Hurricane Earl was formed by the interaction of a tropical wave with an area of cloudiness associated with an upper cold low. At the time of the experiment (1500–2000 UTC) on the 13th, Earl had just begun to recurve and was 1000 km southeast of Bermuda, moving north-northeast at 5 m s^{-1}. Maximum flight-level winds were 50 m s^{-1} and the minimum central sea-level pressure was 983 mb.

The respective satellite and radar images of Earl at the beginning of the rainband patterns (Figs. 4a,b) show the area of study to be 230 km east-southeast of the storm center and oriented north–south, with a crossing angle of 20° from 1630 to 1800 UTC. The crossing angle is defined as the angle between the band axis and a circle concentric to the center of the storm. Two simultaneous crossband patterns, initiated at 1638 UTC, were separated by 70 km (Fig. 4b). At the completion of the crossband pattern, the northern aircraft completed two stepped-descent patterns on the outer side of the band, while the southern aircraft conducted the Doppler pattern northward to where the northern crossband pattern had occurred.

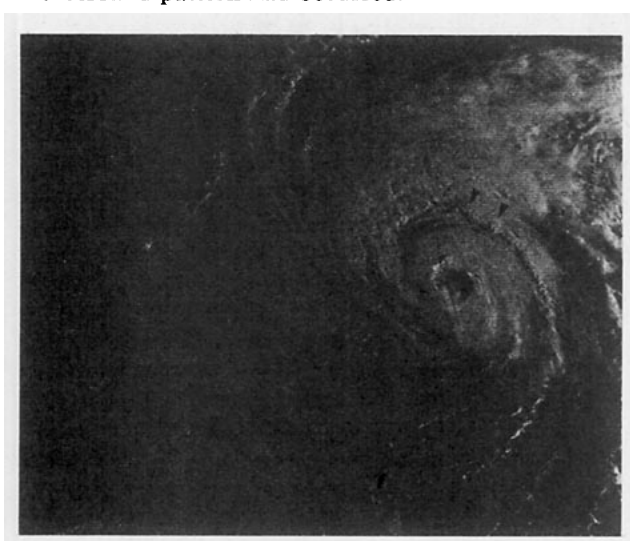

FIG. 3. Satellite photograph of Hurricane Josephine at 1200 UTC 11 October 1984. Arrows denote outer rainband study area.

Satellite (not shown) and radar (Fig. 1) presentations during the last hour of the experiment, indicate that the northern end of the rainband merged with inner secondary rainbands to assume a spiral orientation. The crossing angle at the downband or downwind end increased to 30°. At this point, one aircraft returned to base while the Doppler-equipped aircraft returned to complete the experiment by performing two stepped descents on the inner side of the band from 1920–1950 UTC.

3. Mesoscale rainband precipitation structure

The Josephine and Earl rainbands depicted in the satellite images of Figs. 3 and 4a, as well as those sampled in Hurricanes Debby and Floyd, fit the model of the Stationary Band Complex (SBC, Willoughby et al. 1984) as principal bands. Josephine, Earl, Debby and Floyd showed an open eyewall on the side of the storm opposite the rainband and areas of stratiform precipitation between the eyewall and the principal outer convective rainbands that are similar to secondary bands described by Willoughby et al. (1984).

According to Willoughby et al. (1984), the principal band of the SBC occurs where the Rossby number is of order unity and separates the interior, inertially stable storm core from the outer environment through which the storm is moving. As such, the radius at which the quasi-stationary principal rainband is found may be equivalent to the "effective radius" over which the storm is affected by the environmental "steering" current (Holland 1982). The Josephine and Earl rainbands were ~230 km from the storm center, with Rossby numbers of 1.8 and 1.4, respectively.

a. Determination of rainband location and movement

To identify the rainband edges and track its motion, the band definition employed here is that of BZJM in their study of Hurricane Floyd (1981). The rainband edges were defined by the 25 dBZ contours from the vertical incidence portions of the TA radar sweeps during transects of the aircraft across the band. The positions were also checked by the 30 dBZ contours of horizontal LF radar composites. The axis of the band was determined as the midpoint between the two edges.

The Josephine rainband movement was storm-stationary, despite some inward movement of the inside edge. The outer edge was near stationary (Fig. 5a) and the axis was constant at 225 km in radial distance. The inner and outer edges of the Earl rainband from 1638 to 1810 UTC are given in Fig. 5b. The edges are shown as a function of virtual longitude (storm-relative east–west distance) as determined by vertical incidence tail radar observations from transects of the rainband. Unlike the storm-stationary rainbands of Hurricanes Debby and Josephine, the Earl rainband maintained a significant eastward motion relative to the storm from

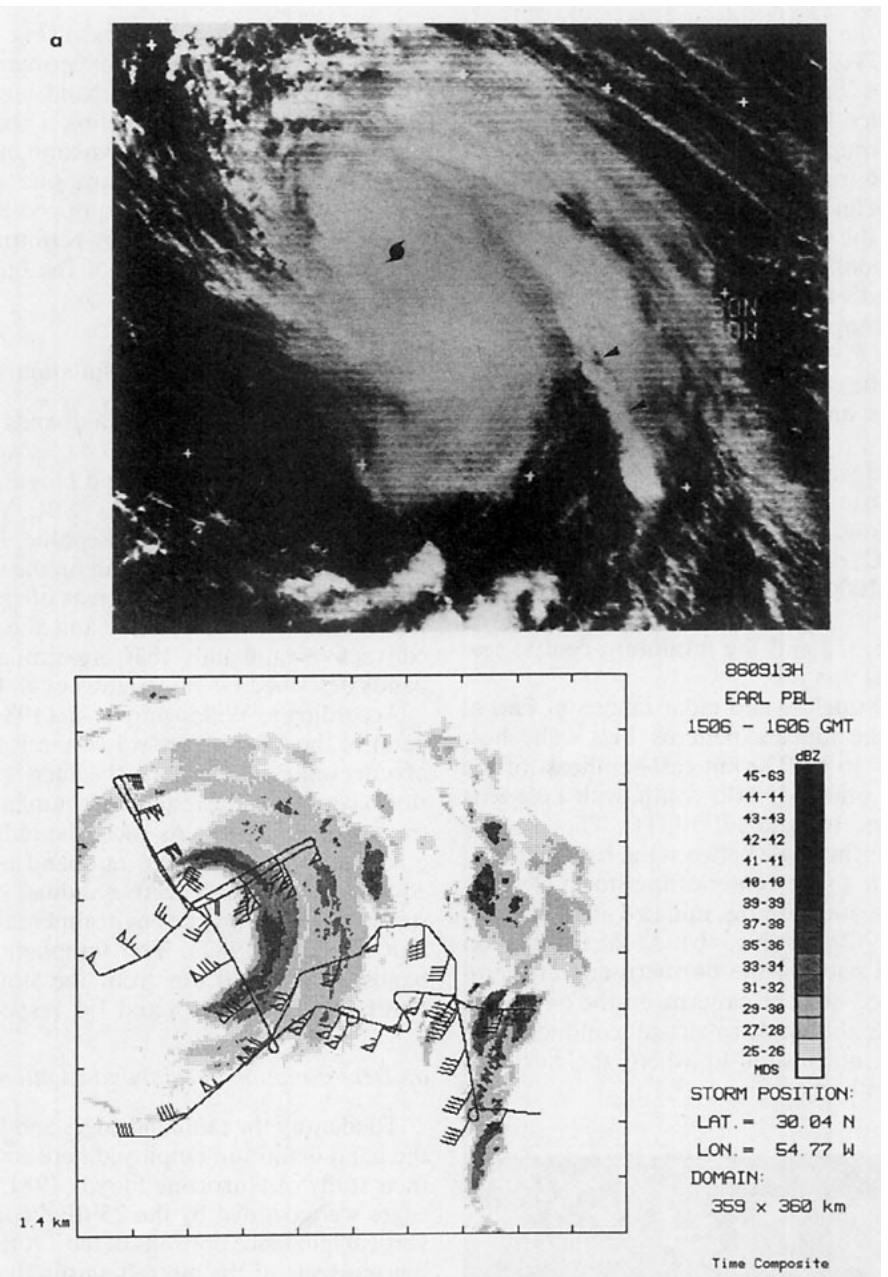

FIG. 4. Hurricane Earl on 13 September 1986. (a) Satellite photograph at 1630 UTC. Filled square indicates storm center, arrows indicate study area. (b) 360 × 360 km LF radar composite for Hurricane Earl. Times and radar reflectivity dBZ scales are indicated on the right. Flight track and wind barbs from 1430–1638 UTC (north part) from aircraft N42RF, and from 1545–1638 UTC (south part) from aircraft N43RF.

1630 to 1800 UTC. The band moved eastward, maintaining its N–S orientation, at 5–8 m s^{-1} at 1645 UTC, decreasing to near zero by 1830 UTC. Shortly thereafter, the band developed an inward spiral (Fig. 1) and no further storm-relative motion was detected during the final hour of the experiment.

A comparison of reflectivity distributions over a 4 h period in Figs. 1 and 4b indicate that, over several hours, the band exhibited a spiral orientation. Determination of the crossband component of this motion was discussed above. The alongband or along-spiral component of band motion was not determined because of difficulties in clearly differentiating between band and cell motions. In addition, the ends of the

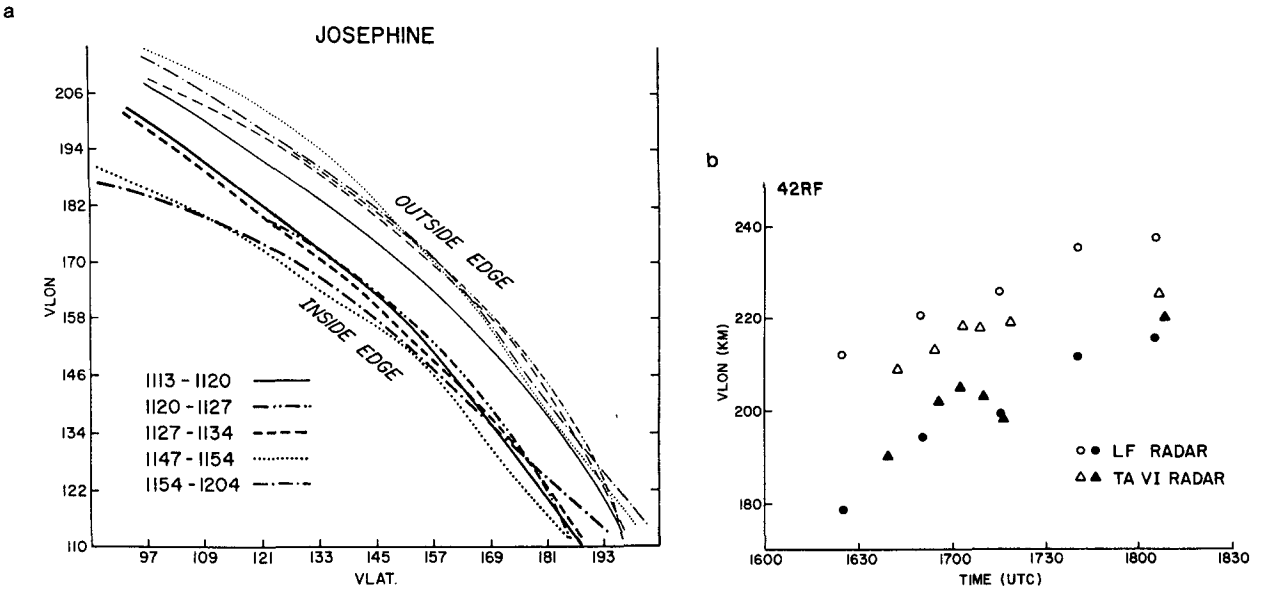

FIG. 5. Rainband inner and outer edge positions. (a) Hurricane Josephine (LF radar) showing storm stationarity. (b) Hurricane Earl (TA and LF radars) for the downband (northern) aircraft, N42RF. LF radar band edges are determined from the 30 dBZ reflectivity contours and TA edges are determined from the 25 dBZ contours. Virtual longitude (latitude) is the storm relative east–west (north–south) component of distance from the center. Open symbols refer to outer side, filled symbols refer to inner side (side closest to storm) of the rainband.

band were not determined because of radar range limitations.

b. Mesoscale precipitation structure and cell movement

The detailed mesoscale and convective-scale structure of hurricane rainbands can be described by small-scale, short-period LF radar composites, such as Fig. 6a for Josephine, or by an individual sweep of the LF radar as shown in Fig. 6b. These figures indicate that the bands were made up of cellular reflectivity elements surrounded by and connected with stratiform rainfall. In Josephine (Fig. 6a), the stratiform precipitation was generally elongated outward from the cells, while in Earl (Fig. 6b), the stratiform rain could be found on either side of the band. Cellular features of >30 dBZ were nearly continuous along the Josephine band axis, with few breaks. Cellular elements in Earl were much more discrete and showed low reflectivity gaps, as long as 12 km, separating cells. Smaller scale (40 × 40 km) tail radar composites and individual sweeps of the LF radar permitted identification and tracking of the cellular features. It was readily apparent that these features underwent considerable changes over the 10 min between radar measurements from each pass. Some of the changes can be attributed to different beam volumes when the aircraft descended to a lower pass level, but changes were also noticeable for consecutive passes at a constant altitude.

Mean cell motion was determined by tracking identifiable features from tail radar composites that were mapped into a storm-relative coordinate system during two consecutive flight legs of the Doppler pattern (at 1500 m level). The time period between consecutive "looks" at a particular cell was 2–10 min. In Josephine, 11 cell motion estimates revealed a mean of 19 m s^{-1} (−1.6 m s^{-1} crossband component and 18.9 m s^{-1} alongband component). Earl provided 37 cell motion estimates with a mean of 17.6 m s^{-1} (0.2 and 17.6 m s^{-1} for the crossband and alongband components, respectively).

Band-relative hodographs constructed from analyses of the airborne Doppler radar wind fields within rainbands in Hurricanes Josephine and Earl are displayed in Fig. 7. Wind profiles representative of the environment adjacent to the bands were not available due to a lack of scatterers. Inflow is restricted to the lower 2 km in Josephine (Fig. 7a) and the lower 3 km in Earl (Fig. 7b). Significant outflow is present above 3 km in Earl and may be associated with the position of the storm southeast of a synoptic scale upper level trough. The band-relative 0.5–5 km shear vector is directed from the inner to the outer side of the band in both cases with 4.7×10^{-3} s^{-1} for Josephine and 3.1×10^{-3} s^{-1} for Earl. The rainbands were both oriented along the density-weighted mean wind for the 0.2–6 km layer. Cell motions were primarily down the band at 80% (Josephine) to 90% (Earl) of the lower tropospheric mean wind. This agrees with the results of cell tracking from landbased radar observations in hurricane Frederic by Parrish et al. (1984).

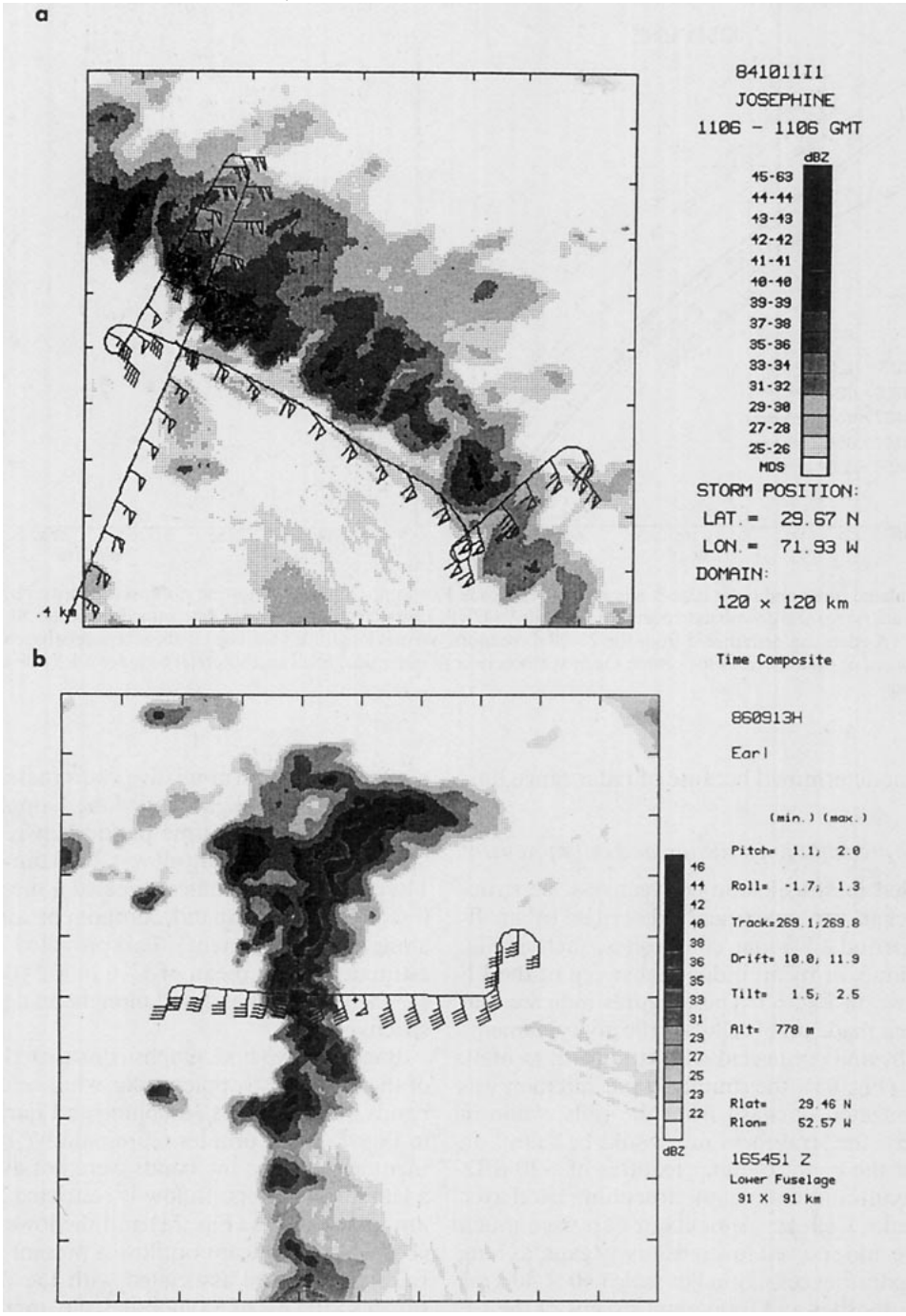

FIG. 6. LF radar presentations of outer rainbands. (a) Hurricane Josephine 120 × 120 km LF radar composite with flight track and wind barbs for 1120–1208 UTC. (b) Hurricane Earl, 90 × 90 km LF radar individual sweep for 1655 UTC. Flight track plotted from 1650 to 1700 UTC.

c. *Vertical cross sections*

In a study of several hurricanes, Jorgensen (1984a) noted that outer rainbands showed a more cellular structure than eyewalls with large alongband reflectivity variations and a tendency for more stratiform rain on the outer side of the band, whereas the eyewall was strongly two-dimensional with a smaller tangential variation of reflectivity and considerable outward slope. Cellular reflectivity elements have been observed in

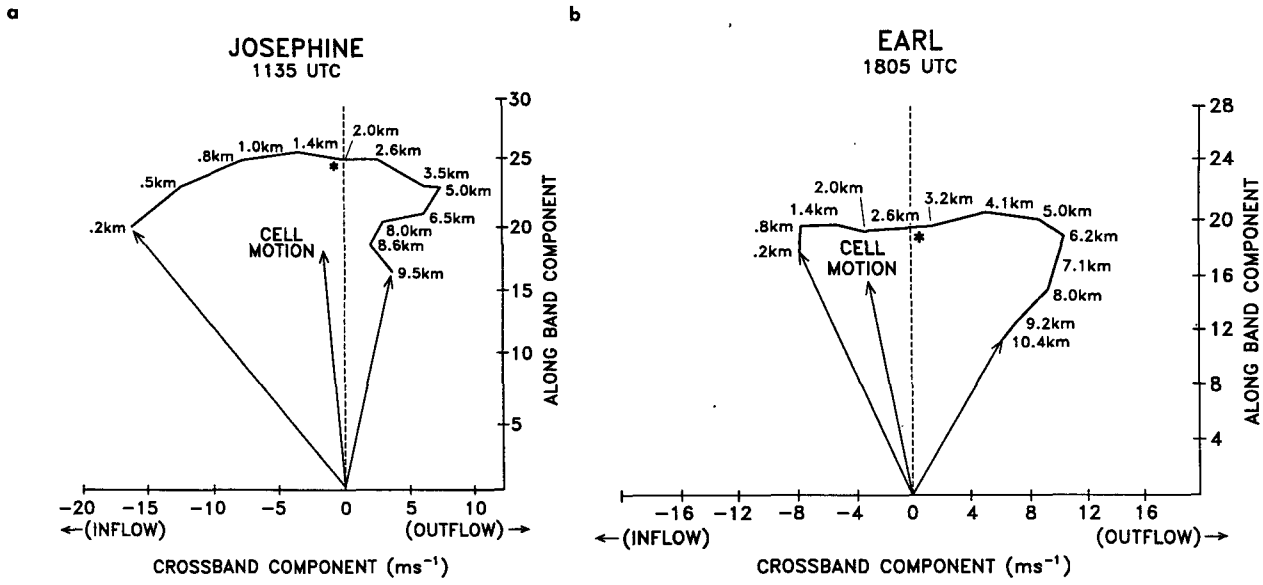

FIG. 7. Airborne Doppler radar-determined, band-relative wind hodographs from 40 × 40 × 10 km analysis regions within the bands. Numbers indicate height of wind in km. (a) Hurricane Josephine at 1135 UTC, (b) Hurricane Earl at 1805 UTC. Asterisks represent density-weighted mean wind from 0.2–6 km.

the hurricane eyewall by Marks (1985), and in outer rainbands by BZJM. They are also similar to the discrete cores of convection or squall-line elements documented by Houze (1977) in his GATE study.

The vertical structure of the Josephine and Earl rainbands, as measured by the tail radar, is presented in Figs. 8a and 8b, which show typical acrossband vertical cross sections. The Josephine section in Fig. 8a is from the flight leg parallel to the band about 8 km on the inner side. The inner edge of the rainband appears as a 6 km high tower. Another cellular reflectivity feature extended outward and up to 8.5 km. Reflectivity gradients were very sharp and maxima were <40 dBZ. A stratiform region of weak horizontal reflectivity gradient was observed at upper levels on the outer side. Occasionally, a poorly defined bright band could be identified near the 4.5 km level. The vertical cross section from Earl in Fig. 8b shows characteristics similar to Josephine, but with stratiform rain on both sides of the axis above 3 km. Occasionally, mamatus were visible on the underside of the anvil above the aircraft. In general, the more intense cellular reflectivity features lie upshear on the inner edge of the bands, while the stratiform rainfall at higher levels extends downshear on the outer side of the bands.

A typical alongband cross section from the tail radar in Earl near the band axis in Fig. 8c shows a predominance of cellular reflectivity features towering as high as 9 km, with some stratiform rainfall above the cells. Alongband sections on the outer side of the bands displayed more stratiform characteristics with a better defined bright-band structure. In some parts of the alongband cross section, there were cellular features that exhibited upband (or upwind) slope with increasing height. This slope was caused by the movement, downband, of the lower part of the cell, with the mean lower level wind (Fig. 7), faster than the upper part of the cell, which had a much weaker alongband motion. A different type of slope (more horizontal) has been found in other hurricane rainbands by Atlas et al. (1963) and Marks (1985). In this type, shafts of stratiform rainfall were generated in cells at higher levels and advected downwind while falling. The BZJM study also suggested that hurricane rainbands display a cellular structure at their upband, or upwind, end and progress to a more stratiform precipitation character farther down the band. This structure was also observed (over alongband distances > 300 km) in Josephine and Earl, but was not evident within the individual study areas.

4. Kinematic structure and dynamics

The organization and development of outer rainbands may be dependent upon larger scale convergence patterns that are produced as a consequence of the motion of the hurricane vortex within its surrounding environment (Ooyama 1982; Shapiro 1983). This forcing often has a preferred orientation relative to the storm center and may be evident as a quasi-stationary, band-shaped low-level convergence region (the SBC of Willoughby et al. 1984). When the forcing is well-organized and a strong convective rainband results, the band-scale updraft must use a portion of the storm

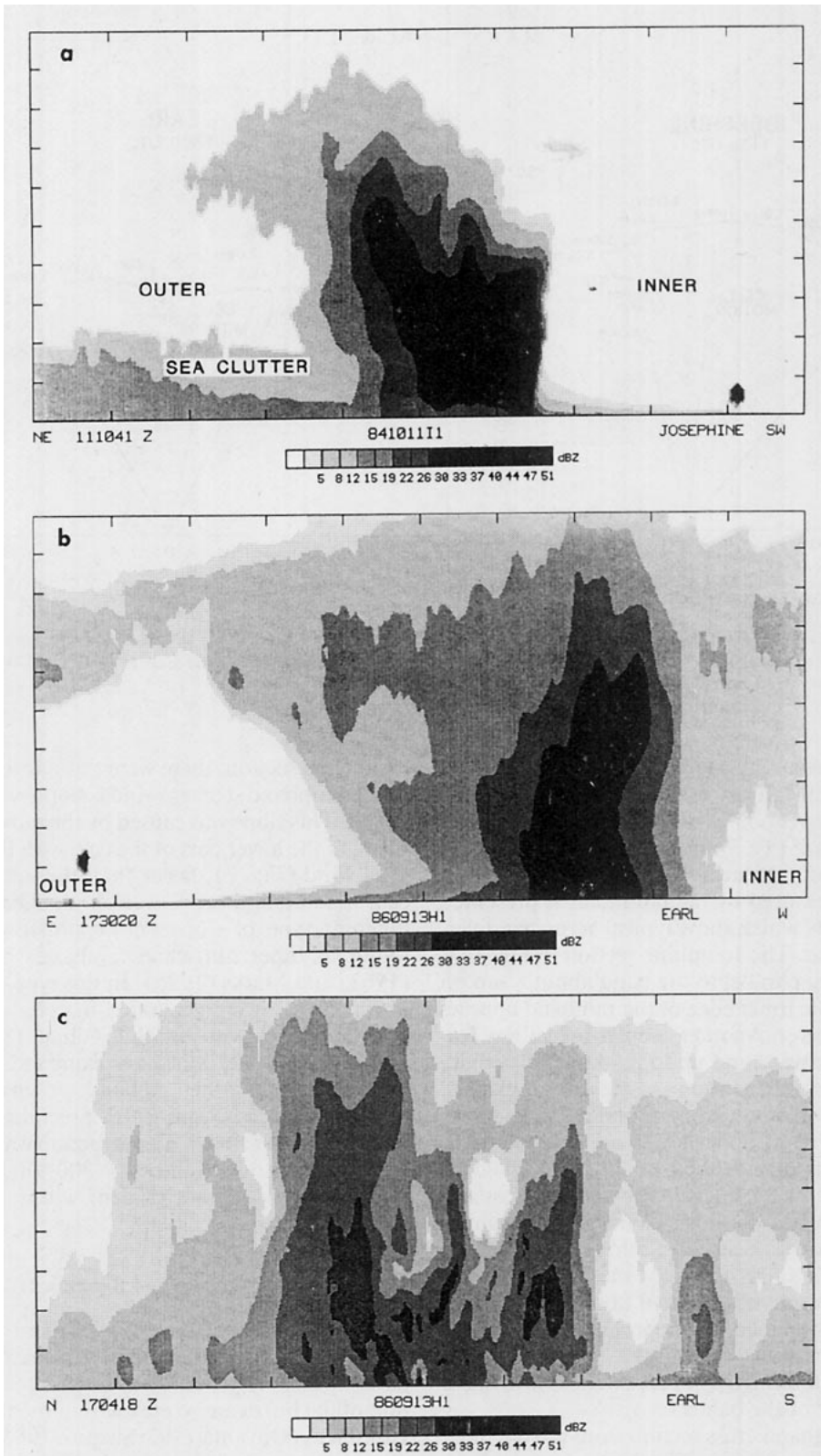

FIG. 8. Tail radar cross sections. (a) Hurricane Josephine for 1110 UTC, height axis tic marks are every 1.2 km, x axis tic marks are every 4 km. Aircraft is at 740 m altitude, heading southeast, 10 km from inner edge of band. Sea surface return (clutter) is shown close to the surface sloping upward with distance from the radar. (b) Same as (a) but for Hurricane Earl at 1730 UTC, x axis tic marks are every 6 km, aircraft at 1500 m altitude heading south on outer side of the band. (c) Alongband radar cross section for Hurricane Earl at 1704 UTC. Tic marks are 1.2 km in height and 6 km on x axis. Aircraft is at 443 m altitude heading into page.

inflow to sustain convection, and an exchange or redistribution of energy and momentum results between the HPBL and the middle troposphere. On the convection scale, this redistribution is evident as updrafts and downdrafts within the individual cells that make up the band. When well-organized within the band, the vertical exchanges of momentum in these drafts allows the rainband to exert a considerable mesoscale influence on the HPBL flow field.

In this section, detailed analyses of reflectivity, flight-level, and vertical incidence (VI) Doppler radar data demonstrate the influence of well-organized rainbands on the two-and three-dimensional kinematic structure and dynamics of the mesoscale flow field in the HPBL for Josephine and Earl.

The rainband-relative wind components in the alongband (V_{alo}) and crossband (V_{cro}) directions are:

$$V_{alo} = V_\theta \cos(\phi) - V_r \sin(\phi) \quad (1)$$

$$V_{cro} = V_r \cos(\phi) + V_\theta \sin(\phi), \quad (2)$$

where ϕ is the band-crossing angle, as defined in Fig. 1. The storm motion (relative to the earth) and band motion (relative to the storm) are subtracted from the measured radial and tangential wind components to give the band-relative tangential (V_θ) and radial (V_r) wind components. All 1-s flight-level data were filtered with a running, 45 s Bartlett filter having a half-power frequency cutoff (frequency where the response function equals 0.5) corresponding to 5 km. This filter preserves mesoscale and the larger convective-scale features and effectively removes smaller scale convective and turbulent fluctuations without changing the phase of significant features. Use of this filter allows comparison with the mesoscale analyses of BZJM and Barnes and Stossmeister (1986), who also used running filter approaches. The Bartlett-filtered data for each band were then sampled and composited with respect to the rainband axis at 2 km intervals of crossband distance, out to 16–24 km (depending upon the length of the leg) on either side of the band axis.

An ideal representation of the rainband would be gained by having several aircraft (one at each level) fly repeated passes across the band while following a particular precipitation element. Compositing these data would tend to smooth out the effects of cells within the element and display mesoscale characteristics. Presenting them as a function of time would provide valuable information on the evolution of the elements and the band. With only one aircraft in Josephine and two aircraft in Earl such a pattern was not feasible. The Hurricane Josephine analyses concentrate on two sections of the band at 500 m while the Earl analyses highlight the HPBL structure of two separate elements within the band at several altitudes. The HPBL experiments were designed to sample individual precipitation elements making up the band without expending too much time, hence some of the convective influences of cells within the elements are present in the mesoscale analyses that follow.

a. Hurricane Josephine

Crossband distance versus height cross sections of the kinematic structure from the first two passes of the Hurricane Josephine rainband are displayed in Figs. 9b–h. The LF radar composite and flight track are shown in Fig. 9a. The plotted reflectivity features in Fig. 9a were composited relative to the moving cell centers over the period of the two transits, 1120–1135 UTC. The cross sections of Fig. 9 are presented in a perspective view as representative of the rainband in the x–z plane (dashed lines) based on one pass at 500 m and one at 1500 m altitude.

The total and alongband winds in Figs. 9b and 9c show strong cyclonic shear across the band, especially at 1500 m, which was caused by a wind minimum just inside the axis and a maximum just outside the axis. The crossband wind component in Fig. 9d shows the most marked inflow (negative values) relative to the storm and rainband at 500 m and extending from the outer side to about 6 km on the inner side of the axis. Since the Josephine rainband was storm stationary, the band and storm relative winds are identical. Maximum convergence (Fig. 9e) is just outside the position of zero inflow, with a divergent region just outside the outer edge of the band at 1500 m. Divergence is computed by assuming a two-dimensional flow structure with no alongband variation of the wind,

$$\text{div} \approx (\partial V_{cro}/\partial x) + (V_{cro}/R), \quad (3)$$

where x is the crossband distance (km) and R is the radial distance from the storm center. We have neglected the second term, which is over an order of magnitude smaller than the first and changes little across the band. The Bartlett-filtered vertical wind component (Fig. 9f) shows maximum upward motion of 2–3 m s^{-1} at the position of maximum crossband convergence. Downward motion is just inside the zero inflow line on the inner side of the band and 14 km outside the band axis. It is coincident with the area of positive crossband divergence. The cyclonic shear across the band results in maximum relative vorticity (Fig. 9g) on the band axis at the 1500 m level. Relative vorticity was computed by assuming two-dimensionality with no alongband variation of the crossband wind component,

$$\zeta \approx (\partial V_{alo}/\partial x) + (V_{alo}/R). \quad (4)$$

The second term is an order of magnitude less than the first, varies little across the band and is neglected. In hurricane studies, the storm-scale radial pressure profile is often shown as a profile of the D-value, which typically exhibits an increase with distance from the

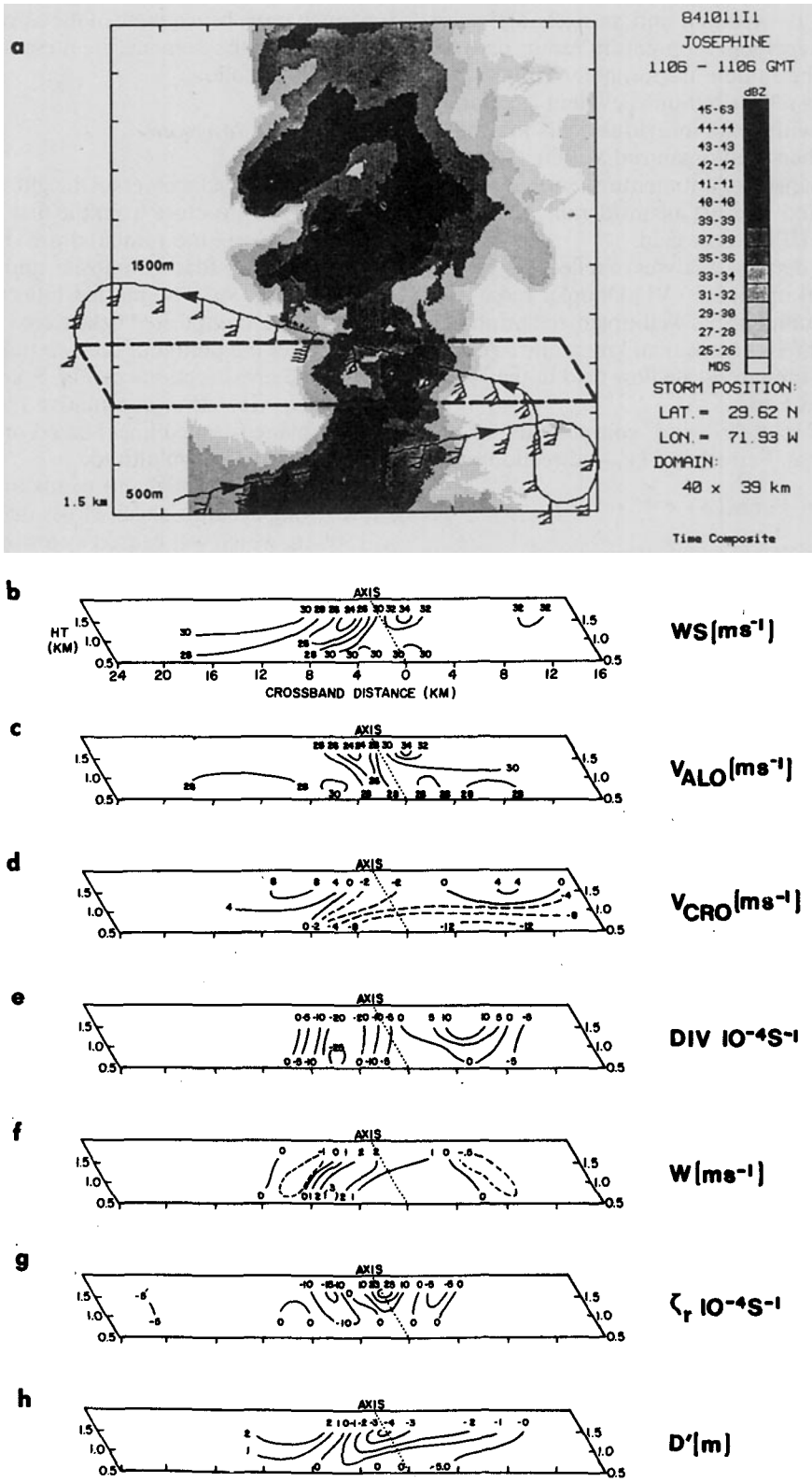

FIG. 9. Crossband fields in Hurricane Josephine. (a) 40 × 40 km LF radar composite for Josephine at upband end (top of page is 320° relative to north). Perspective analyses of 1500 and 500 m levels for dashed area of (a). *X* axis is height and *Y* axis is crossband distance (0 = band axis). (b) band-relative windspeed, (c) alongband wind component, (d) crossband wind component, (e) divergence, (f) vertical wind, (g) relative vorticity and (h) *D*-value perturbation.

storm center. Rainband influences often show up in the storm-scale D-value profile as a flattening and/or dip in the profile of a few meters (see Powell 1987 and Barnes and Stossmeister 1986 for examples). The rainband-scale pressure perturbation was estimated by computing the deviation of the actual D-value profile from a linear least-squares fit of the profile taken from equal distances (~20 km) on either side of the rainband. This rainband-scale effect on the pressure field is presented as the perturbation D-value field, D', in Fig. 9h. The pressure minimum associated with the band is about 4 m (~0.4 mb), which is about the same order as the pressure departure of a line of tropical cumulonimbus (from 500 m to 3 km altitudes) documented by LeMone (1983). LeMone found that the mesoscale pressure perturbation minimum was produced hydrostatically by condensation heating, but felt that dynamic pressure effects (interaction of the updraft with the wind shear as described by Rotunno and Klemp (1982) were important on the convective-core scale. More recently, LeMone et al. (1987) found similar pressure perturbations in midlatitude convection.

Two crossband transits, made 80 km farther down the band at the 500 m level, are presented in Figs. 10a–h. The rainband relative wind analyses in Figs. 10b–d are similar to those that would be expected from Figs. 9b–d, except that the horizontal shears are stronger. Maximum total and alongband winds are on the outer side of the rainband axis; there is a pronounced wind minimum 6–8 km on the inner side. The crossband winds in Fig. 10d show the low-level flow converging toward the inner edge of the band from both sides. The crossband component of the divergence (Fig. 10e) again shows a strong convergence maximum of -4×10^{-3} s^{-1} between the band axis and the zero line of the crossband wind component. The vertical wind component in Fig. 10f shows upward motion of 1–3 m s^{-1} on the inner side of the rainband axis with downward motion of up to 2 m s^{-1} associated with a divergence maximum on the band's inner reflectivity edge. The D' field in Fig. 10g shows a minimum at, or slightly inside of, the axis of ~0.8 mb. The relative vorticity maximum (Fig. 10h) in this case is coincident with the convergence maximum that is 4–6 km to the inside of the rainband axis. Although Fig. 10 shows some alongband variability of the kinematic quantities, there is a strong two-dimensional signal across the rainband similar to that displayed in Fig. 9.

As shown in Fig. 11, the inner edge of the band is the preferred side for convective-scale drafts. Drafts are defined as vertical motion with a magnitude ≥ 1 m s^{-1} for a flight track distance of >1 km as deduced from the time series of unfiltered 1 s data from all the crossband transits. The four transits of the Josephine band measured 19 drafts that comprised 13 updrafts (68%) and 6 downdrafts (32%). The peak updraft frequency was at the band axis, while the peak downdraft frequency was 10 km on the inner side of the axis.

Despite the sampling of some strong downdrafts (−7 m s^{-1}) during the profiles across the band, no evidence of larger scale (10 km) downdraft spreading was found. Hence, as developed in Part II, no low equivalent potential temperature (θ_E) air was found of the type observed in Floyd by BZJM. This is probably a sampling problem rather than a lack of spreading downdrafts. The aircraft never flew below 500 m during the crossband profiles or below 140 m during the stepped-descent profiles adjacent to the inner side of the rainband. Stepped-descent profiles (not shown) indicated constant vertical wind shear of 0.01 s^{-1} from 140–1500 m in the crossband component and strong shear (0.025 s^{-1}) below 500 m in the alongband component due to the strong stability caused by cool sea surface temperatures of 24°–24.5°C. Cold-spreading downdrafts, especially in stably stratified conditions, are probably very shallow and may have been present below flight level. This possibility caused the experiment to be redesigned for Hurricane Earl to allow simultaneous crossband profiles by two aircraft at levels as low as 150 m and stepped-descent profiles down to 80 m.

The analyses of Fig. 9 highlight the quasi-two-dimensional structure of the Josephine rainband. A comparison with Fig. 10 shows that the 500 m level flow may vary considerably in the alongband direction. Although few observations were available far enough on the outer side of the band to be considered the typical or "undisturbed" HPBL, these analyses indicate that the Josephine rainband produced a considerable perturbation in the HPBL flow field. The rainband enhanced the cyclonic shear across the band. A wind velocity minimum and maxima of convergence, vertical motion, and relative vorticity were a few kilometers to the inner side of the rainband reflectivity axis, and a D-value (pressure) minimum at the axis and the wind maximum were just outside the axis.

b. Hurricane Earl

More detailed measurements of the two-dimensional structure of the HPBL were gathered in Hurricane Earl. These measurements were gathered in simultaneous crossband profile patterns, which were 70 km apart along the rainband, and in airborne Doppler-radar flight patterns, all of which attempted to follow particular cellular reflectivity elements. The prominent characteristics of this structure were most evident during the crossband profiles conducted at the northern end of the rainband. Complete details on the profiles from the southern end of the rainband and the Doppler patterns are available in Powell 1988.

1) REFLECTIVITY CROSS SECTIONS AND CELL EVOLUTION

The tail radar horizontal reflectivity composites for the 1500 m level and vertical incidence (VI) cross sec-

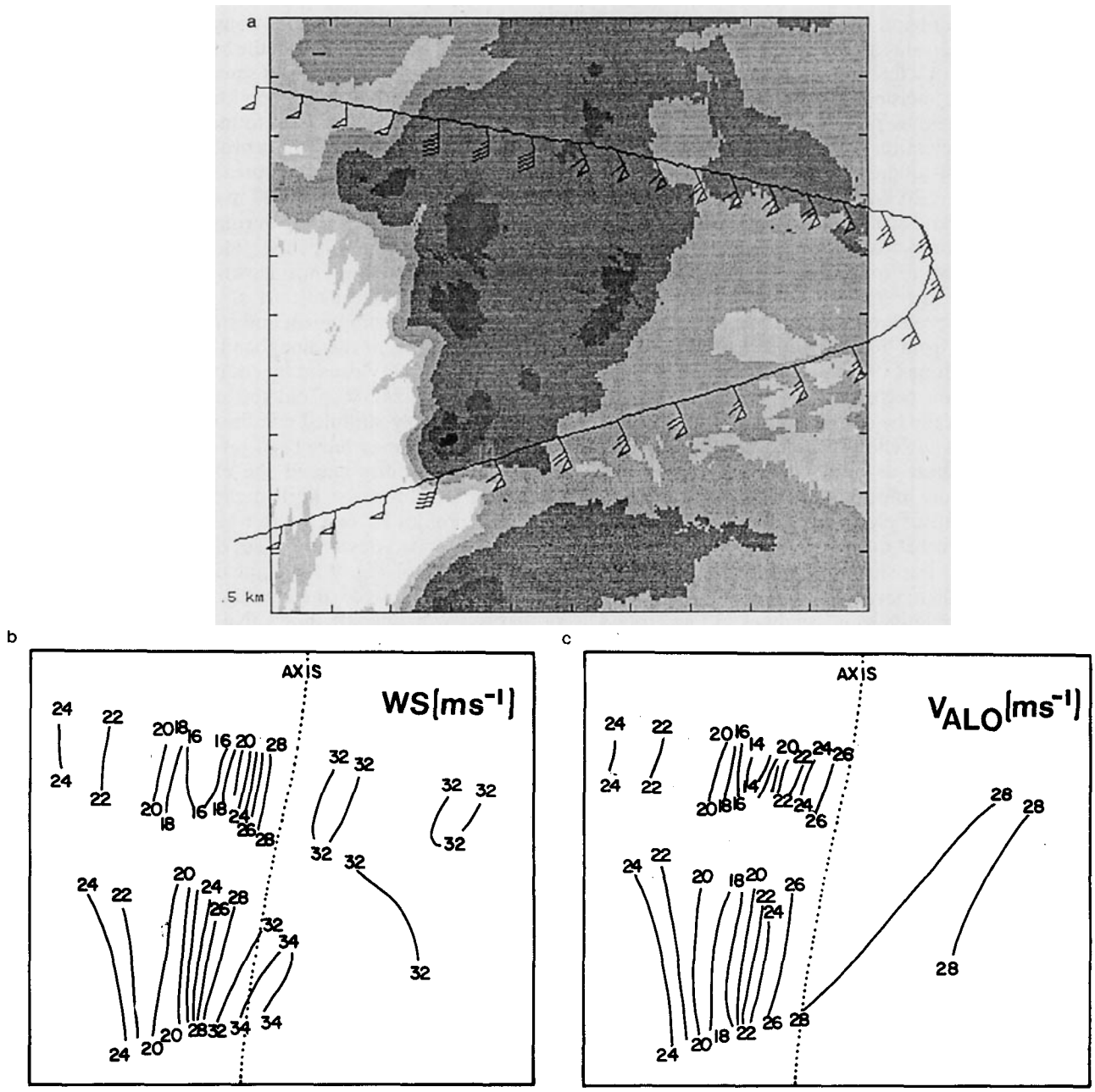

FIG. 10. As in Fig. 9, except plan view of 500 m level data at downband end (top of page is 300° relative to north), (g) is *D*-value perturbation, and (h) is relative vorticity.

tions for each of the downband (north) transits of the band are depicted in Figs. 12a–j. The horizontal plan view TA radar analyses show the proximity of the aircraft flight track relative to the cellular reflectivity elements composited over an 8–10 min period; the VI cross sections depict the near-instantaneous reflectivity experienced above the aircraft during the transit.

The northern aircraft (42RF) sampled the middle portion of a Y-shaped precipitation element (defined as an aggregate of imbedded, short-lived reflectivity cells that maintains its shape or identity over time scale of 0.5–1.5 h) at successive levels of 1350 m (Fig. 12a,b), 770 m, 450 m, 260 m (Fig. 12c,d), and 150 m (Fig. 12e, f), from 1638 to 1721 UTC. Even though the aircraft came close to sampling the same part of the band during each pass, the radar view of the rainband in Fig. 12 underwent considerable evolution from pass to pass because of temporal changes and changes in the radar

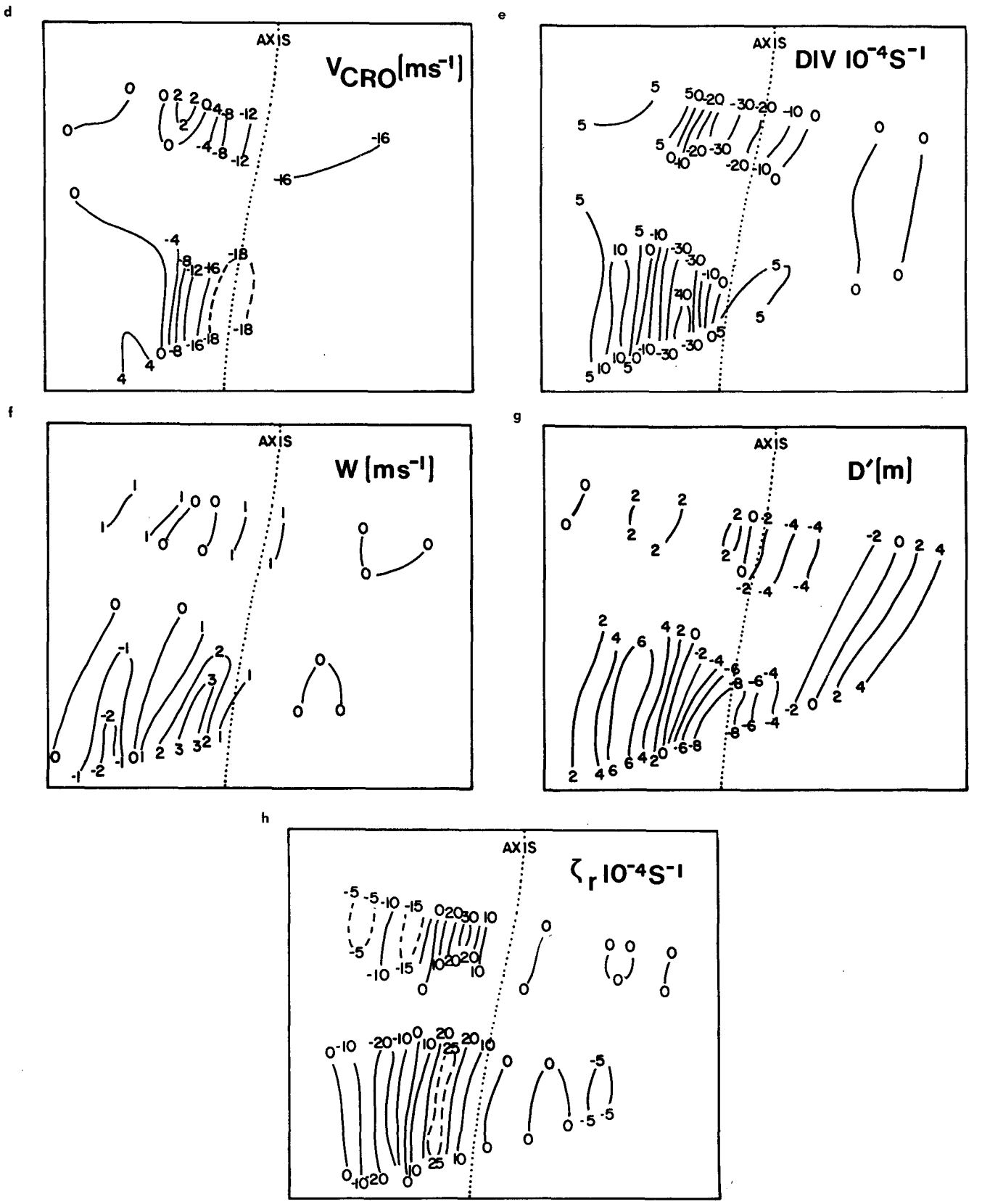

FIG. 10. (*Continued*)

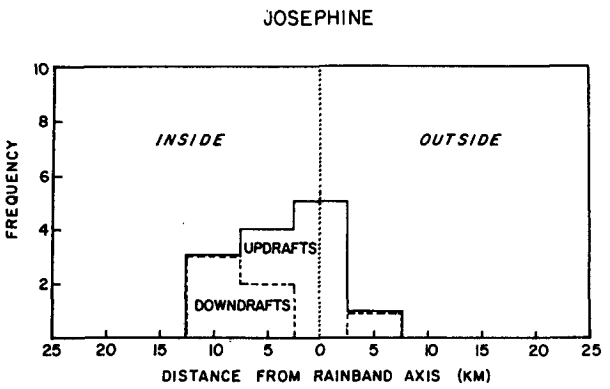

FIG. 11. Histogram of drafts with magnitude > 1 m s^{-1} for 1 km or more of crossband flight track for Hurricane Josephine. Frequency is total number of drafts per 5 km interval of crossband distance.

sampling volume as the aircraft transected at different levels. Although the general (Y pattern) shape of the element was maintained throughout the ~45 min required for the profiles, the individual cellular reflectivity maxima within it were rarely identifiable for more than 15 min.

These time scales compare with results of land-based radar cell tracking performed by Parrish et al. (1983) for Hurricane Frederic (1979) and recent land-based radar movies produced by scientists at the Hurricane Research Division in 1988. In general, they found a hierarchy of rain areas with small cells having 6–10 min time scales with areas of 10–100 km^2, and mesoscale bands or elements with lifetimes of 45–90 min and areas of ~100–1000 km^2. Land-based radar analyses and movies indicate that new cells tend to form on the upband or upwind end of the band and then grow in area and intensity while moving down the band. The radar data analyzed here do not indicate any preference for cell formation on a particular side or end of the rainband.

The Y-shaped precipitation element consists of several individual cells, ~10 km in diameter, extending 7–10 km in height and having some indication of outward tilt and stratiform extension of reflectivity toward the outer (east) side. Some indication of stratiform rain is shown in Fig. 12b on the outer side of the band where observers noted a well-defined anvil cloud (with mamatus underlying) farther down the band (eastern extension of the Y). This stratiform region was also observed following the final transit of the crossband pattern shown in Fig. 12e,f. Three of the five VI reflectivity cross sections (e.g., Figs. 12b,d) show cellular reflectivity maxima of >35 dBZ on the inner side of the band axis and two (e.g., Fig. 12f) display maxima that are closer to the axis. The wind barbs (earth-relative) plotted on the flight tracks across the band often show generally alongband flow with significant confluence wind shifts near cellular reflectivity features (Figs. 12a,e). At the 150 m level (Fig. 12e), a large-scale (20 km) diffluent wind pattern is evident on the inner side of the band.

2) KINEMATIC STRUCTURE

The composite kinematic structure of this precipitation element throughout the 43 min of the crossband profiles (Fig. 2b) is shown in Figs. 13a–f. The rainband-relative winds in Figs. 13a,b show wind maxima of 8–10 km on the outer side of the band axis for the three wind components. Wind minima occur 6–8 km on the inner side of the band axis for V_{cro} (Fig. 13a) and at 20 km for V_{alo} (Fig. 13b). Double wind maxima are present at the 1350 and 450 m levels at locations corresponding to double reflectivity maxima (e.g., Fig. 12b). The lack of double maxima on other passes of the same element is associated with the time dependent and three-dimensional characteristics of the reflectivity and flow fields as individual cells evolve within the element. These analyses show strong cyclonic shear across the band, with the highest winds at the 500–1000 m level. Negative values of V_{cro} throughout the band show that the inflow continues across the rainband axis from outside to inside.

Maximum convergence of -10×10^{-4} s^{-1} (Fig. 13c) occurs 2–10 km on the inner side of the axis. At low levels (<260 m), on the inner side of the band axis, a large-scale divergence maximum is found in the region of diffluent flow, which is shown in Fig. 12e. The vertical velocity (W), maxima (Fig. 13d) are well correlated with the maxima in the convergence field. Maximum upward motion is >4 m s^{-1} at the 1350 m level, and significant downward motion is 8 km from the axis on both sides of the band, especially below 450 m on the inner side. Double maxima of W are seen at the 1350 m level, near the double reflectivity maximum (Fig. 12b). Vertical velocity maxima are slightly inward of the rainband axis, except for the 260 m level transit, which is dominated by downward motion, and the 150 m level transit, which shows maximum upward motion on the outer side of the band axis.

The lower two levels of the northern crossband profiles show evidence of a downdraft centered about 12 km to the inner side of the band axis. At 260 m, downward motion occurred in a region of crossband convergence indicating that the alongband (unmeasured) component of the divergence was important. The large positive divergence and diffluent flow at 150 m indicate that the downdraft is spreading out at this level. The time and space scales of the 260 m level downward motion and 150 m level diffluence suggest a band-scale (20 km) downdraft on the inner side of the rainband. This downdraft region is the subject of further examination in Part II.

The D' field (Fig. 13e) shows negative values throughout the area within 10 km on either side of the

band axis. Maxima in the D' field occur farther than 10 km from the band axis on both sides. There is a secondary maximum on the inner side at 260 m and positive values are closer to the band axis at 150 m where the above-mentioned downdraft is spreading out. The vertical component of the relative vorticity (as computed by (4)) in Fig. 13f shows maximum values near the band axis at the 1350 and 150 m levels, a vertical alignment of positive relative vorticity near the band axis, and double maxima at 1350 m.

Although not as marked as at the downband (north) end of the band, a mesoscale two-dimensional structure was also apparent from simultaneous crossband profiles conducted 70 km to the south (details in Powell 1988). The similarity of the kinematic analyses of the Earl profiles and their comparison with Hurricane Josephine, is encouraging. Common features include: 1) strong cyclonic shear across the band, with maxima of V_{alo} and V_{cro} on the outer side of the band axis and minima on the inner side; 2) upward vertical velocity and convergence maxima on the inner side of the axis; and 3) D-value minimum found at the band axis. These cases suggest that well-organized, outer convective rainbands satisfying the Willoughby et al. (1984) general criteria of the stationary band complex model (i.e., quasi-stationary principal rainbands that persist on one side of a storm) have common precipitation, kinematic, and thermodynamic characteristics that imply similar convective-scale and mesoscale dynamics.

3) Convective drafts from all crossband legs

Draft frequencies for the 14 crossband profiles in Fig. 14 indicate that the most significant vertical motion occurs in cells on the inner side of the rainbands axis. Of 38 measured drafts, 23 (60%) were updrafts and 15 (40%) were downdrafts. The strongest drafts were within 5 km of the rainband axis. These updraft and downdraft percentages are very close to those in Josephine (68%, 32%) and Hurricane Floyd, where BZJM found 63% and 37% respectively.

4) Stepped-descent wind profiles adjacent to the band

Stepped-descent profiles (Figs. 2a,c) of the along- and crossband wind components are presented in Figs. 15a and 15b, respectively. Two profiles made parallel to the rainband on the outer side from 1730–1801 UTC were combined to form profile "O," representative of the HPBL 40 km to the outer side of the band axis. The I1 profile was made from 1916–1929 UTC on the inner side of the band, 15–20 km from the axis, while the I2 profile was made from 1932–1945 UTC further (30–40 km) for the axis. The outer side V_{alo} profile shows a logarithmic shape and relatively weak winds. Maximum V_{alo} winds are shown in I2 since it is closest to the storm center (180 km). All profiles show weak vertical wind shear in V_{alo} above 500 m and stronger ($0.015\ s^{-1}$) shear below. The V_{cro} profiles exhibit near-constant shear ($0.005\ s^{-1}$) in the crossband component from 80 m upward for profiles O and I2. An interesting feature in these profiles is the apparent sampling (in profile I1) of a gust front spreading out at low (altitude < 400 m) levels from the band axis toward the (nearly rain-free) inner side of the rainband. A low-level wind maximum at the 80 m level is especially apparent in the crossband flow in Fig. 15b. Further evidence of this feature (from the airborne Doppler radar) will be presented in the companion paper (Powell 1990).

The gust front detected in profile I1 is similar to the spreading downdraft discovered during the northern crossband profile discussed in section 4b(2). In addition, VI Doppler radar cross sections through the band at 1802 UTC, showed downdrafts extending to the surface on the inner side of the band. These data illustrate a predominance of downdraft spreading near the surface on the inner side of the rainband axis. These occurrences and evidence from BZJM indicate that hurricane rainbands do occasionally possess downdrafts that are capable of spreading out at low levels, and that such downdrafts may be too shallow (<500 m) to be detected in many cases.

5) Synopsis of the Earl rainband kinematic structure

The life cycles of two major precipitation elements making up a portion of an outer principal rainband in Hurricane Earl were followed for 1.5 h. The bulk of the crossband profiles pertain to a period during which the rainband moved perpendicular to its orientation (eastward) at 5 m s^{-1}. Each precipitation element comprised several reflectivity cells that were moving parallel to the band axis in the direction of the lower tropospheric (density-weighted) mean winds. These cells displayed a convective structure at the axis of the rainband with the 25 dBZ reflectivity contour height reaching 7–9 km. A more stratiform, anvil type of rainfall was present on the outer side of the axis. The convective cells were developing, maturing and decaying over periods of ~15–30 min.

Aircraft sampling of the rainband's kinematic structure resulted in 14 crossband flight legs and 4 alongband profiles. Mesoscale filtering of the crossband profiles yielded a consistent two-dimensional structure. Differences in individual profiles were evident as lack of vertical continuity in the crossband analyses from pass to pass. This occurred because the mesoscale filtering process does not remove the influence of the largest convective scales. Hence, the crossband analyses contain some alongband (three-dimensional) and vertical variability in structure that was produced by the evolution of individual convective cells within each precipitation element.

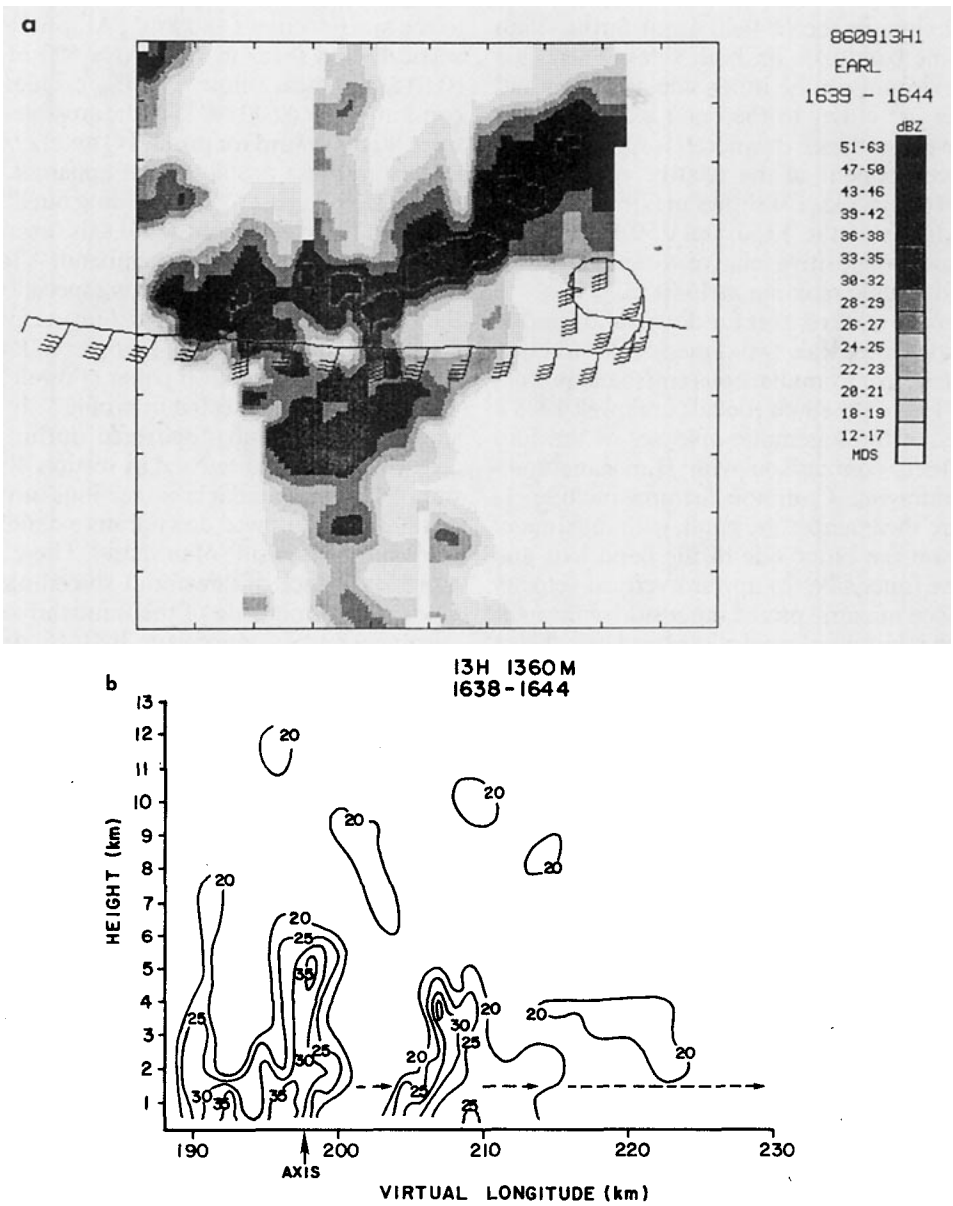

FIG. 12. Tail radar 50 × 50 km plan view composite and VI cross section pairs for Hurricane Earl crossband patterns at the downband (northern) end (top of page is due north) of the rainband. (a) origin at V_{long}, V_{lat} (in km east and south of storm) of (185, −90), (c) (185, −80), and (e) (185, −70).

5. Conceptual model of rainband kinematic and precipitation structure

The similarity of the two-dimensional mesoscale and convective-scale structure of the Josephine and Earl rainbands allows summarizing their kinematic and precipitation structures with a schematic model (Fig. 16) that represents a well-organized outer convective hurricane rainband. The plan view (Fig. 16a) is appropriate for any level below 1600 m (maxima and minima may be shifted for tilted updrafts). The rainband cross section (Fig. 16b) cloud edge (shaded border) and reflectivity pattern (solid contours) are based upon the VI TA radar cross sections and cloud liquid water measurements. Horizontal arrows depict the crossband component of the wind from the airborne Doppler radar (arrows at left side of figure at 1, 3, 5, 7, and 10 km) and from flight-level measurements at 1500 and 150 m levels. The perturbation pressure minimum is located at the rainband axis (defined as the midpoint between 25 dBZ contours). Minimum V_{alo} and V_{cro} are found on the inner side of the axis, as are most cellular reflectivity maxima, maximum

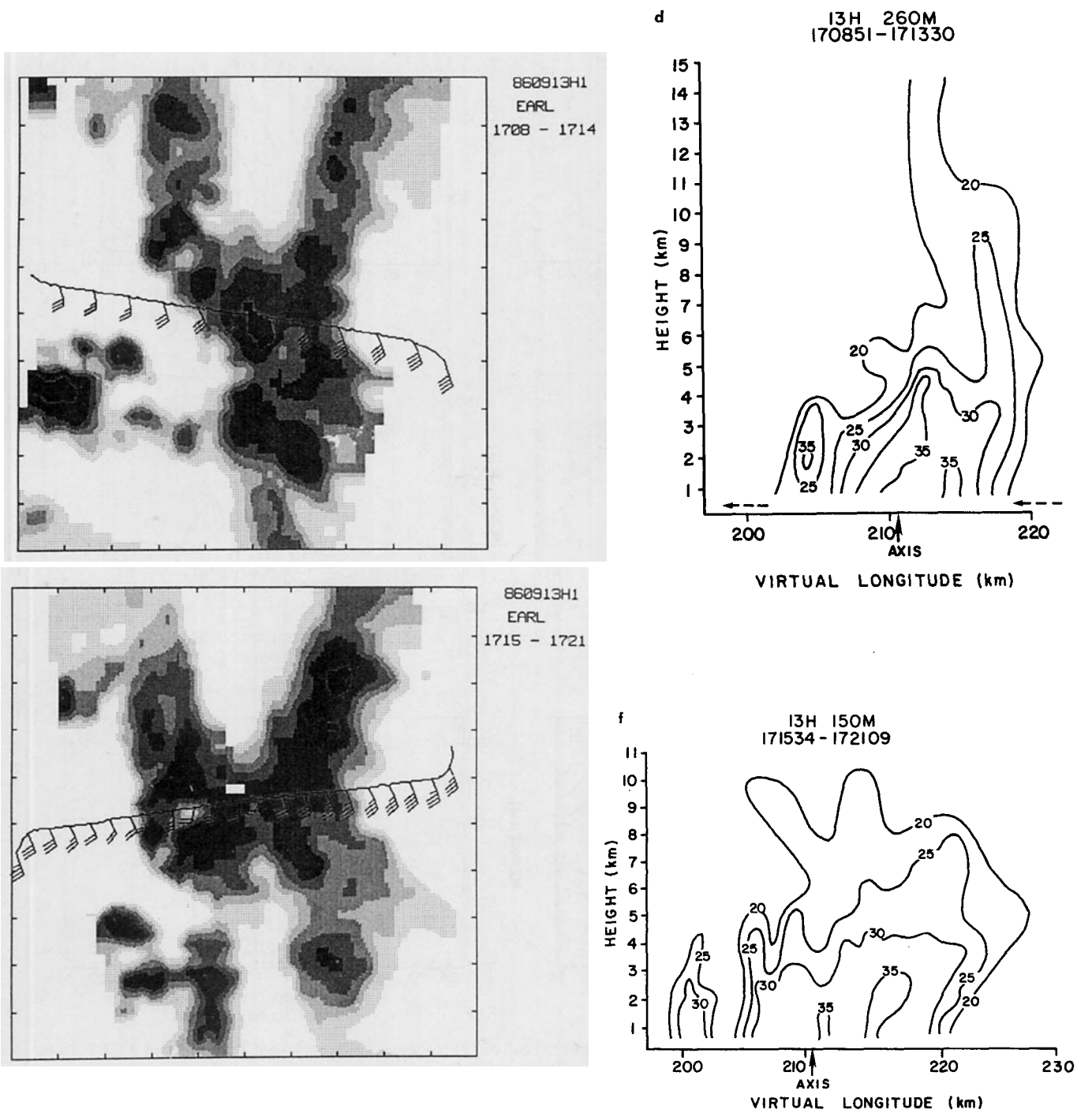

FIG. 12. (*Continued*)

convergence and maximum relative vorticity. Most updraft and downdraft cores were located in the region of maximum reflectivity on the inner side of the band. Bold arrows depicting an updraft and a spreading downdraft are collocated in this region, but do not necessarily occur at the same time, since most of the drafts (60%–70%) are updrafts. Maximum V_{alo} and V_{cro} are found on the outer side of the axis, as is stratiform rain falling from the anvil. The wind shear vector above the HPBL is directed from the inner side to the outer side such that the stronger reflectivity cells and the updraft axis are found on the upshear side of the band and show some indication of downshear tilt. The stratiform precipitation extends downshear as anvil rain,

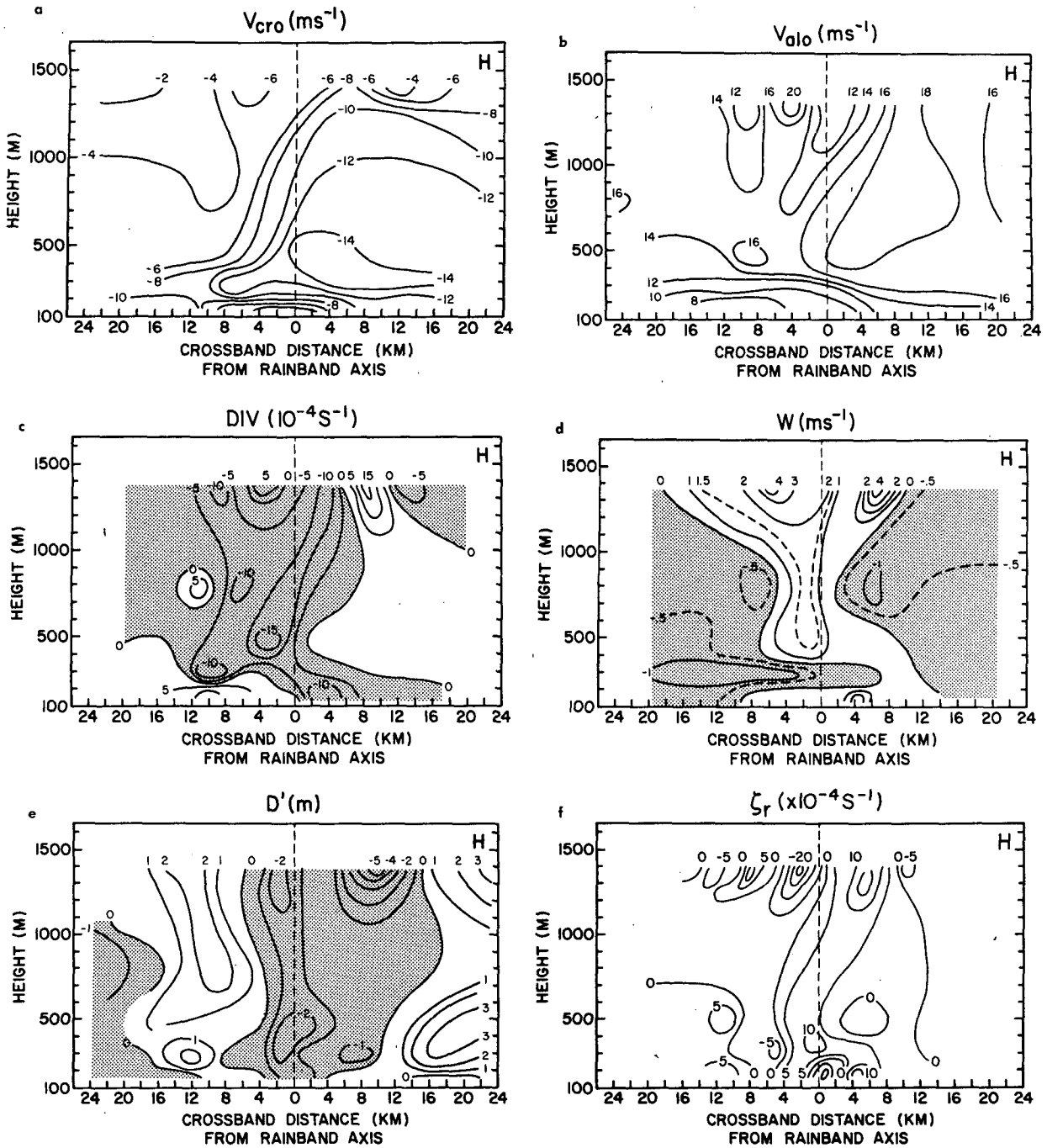

FIG. 13. Crossband profile analyses at downband (northern) end of: (a) crossband wind component, (b) alongband wind component, (c) divergence, (d) vertical wind component, (e) *D*-value perturbation, (f) relative vorticity.

with some anvil also present on the upshear side. Some of the anvil showers are strong enough to generate penetrative downdrafts (vertical arrows beneath the inner side anvil). Divergence maxima may be found on either side of the band, clear of the convective activity, and suggest mesoscale compensating subsidence (small vertical arrows beneath the outer side anvil).

The Floyd rainband (BZJM) and the Irene rainband described by Barnes and Stossmeister (1987) have many of these characteristics, but they were so close (at 75 km) to the eyewall that the vortex-scale storm structure may have masked some of the rainband mesoscale kinematic features, especially on the inner side of the bands.

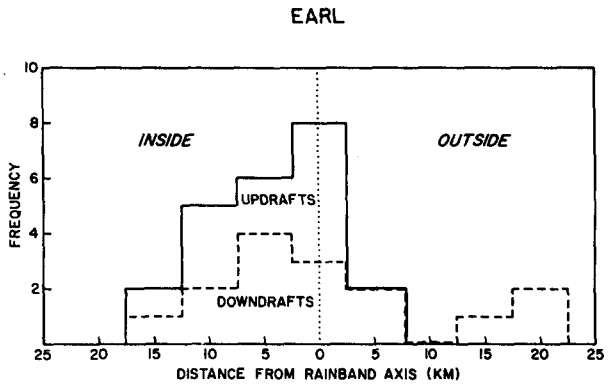

FIG. 14. As in Fig. 11, except from 14 crossband flight legs in Hurricane Earl.

Many of the above features were also evident in analyses of the mesoscale and convective scale structure of the eyewall made by Jorgensen (1984a,b). He also investigated outer rainbands, but found an absence of a pronounced tangential wind maximum and consistent updraft, except in an outer convective ring (a double eyewall on 8 August 1980 in Hurricane Allen). His composite profiles mainly contained data that were collected above the HPBL (from 1500 m or above). Although not as prominent as the eyewall, the relative positions of anomalies in the tangential, radial and vertical winds and divergence in an outer rainband in Hurricane Anita (1977) are in similar positions to those indicated by the Josephine and Earl analyses. In addition, his composite profiles for the eyewall from Hurricanes Anita, Frederic (1979) and Allen (1980) indicated a prominent updraft maximum 3–4 km to the inner side of the tangential wind maximum and maximum radial inflow on the outer side. A major difference is that the tangential wind maximum in the eyewall tilted strongly outward on the inner side of the maximum eyewall reflectivity, while the Josephine and Earl rainbands exhibited little or no tilt and had wind maxima on the outer side of the rainband axis. These comparisons indicate that well-organized outer rainbands have a definite effect on HPBL structure and may have characteristics that are similar to those of the eyewall.

6. Dynamic aspects of the Josephine and Earl rainbands

The characteristic features of an outer convective rainband's kinematic structure have dynamic associations that may help to explain the cause of the perturbation pressure field, the cyclonically sheared wind field across the band and vorticity generation in the band.

The rainband pressure minimum has been observed by many investigators, but its position with respect to band reflectivity features has been unclear. The perturbation pressure minima observed in Earl and Josephine were clearly defined on 17 out of 18 crossband flight legs. On 9 transits the D-value minimum was on the outer side of the updraft, on 2 it was on the inner side and on 1 leg it was coincident. In 6 transits, the phase relationship could not be determined because of a flat D-value perturbation field or no prominent updraft. This D-value perturbation minimum is very similar in magnitude to the mesoscale pressure departure field observed by LeMone (1983) in a GATE rainband and quite recently by LeMone et al. (1987) in midlatitude convection. An example of the perturbation pressure minimum and its position relative to the updraft core and band edges is presented in Fig. 17 from the 1600 m level crossband profile at the

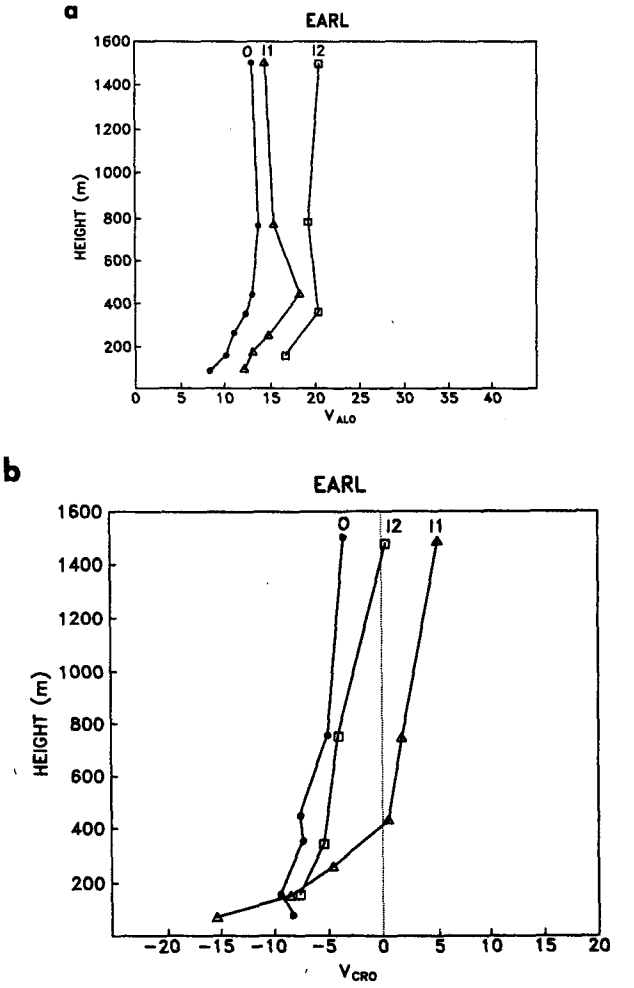

FIG. 15. Vertical profiles from stepped-descent patterns on outer (O) and inner (I1, I2) sides of the Earl rainband, (a) Alongband wind component, (b) crossband wind component.

a

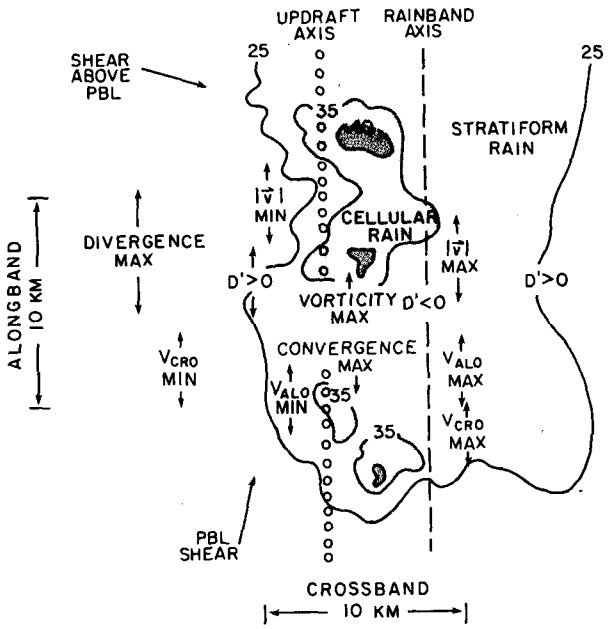

RAINBAND KINEMATIC STRUCTURE

b

RAINBAND KINEMATIC AND PRECIPITATION STRUCTURE

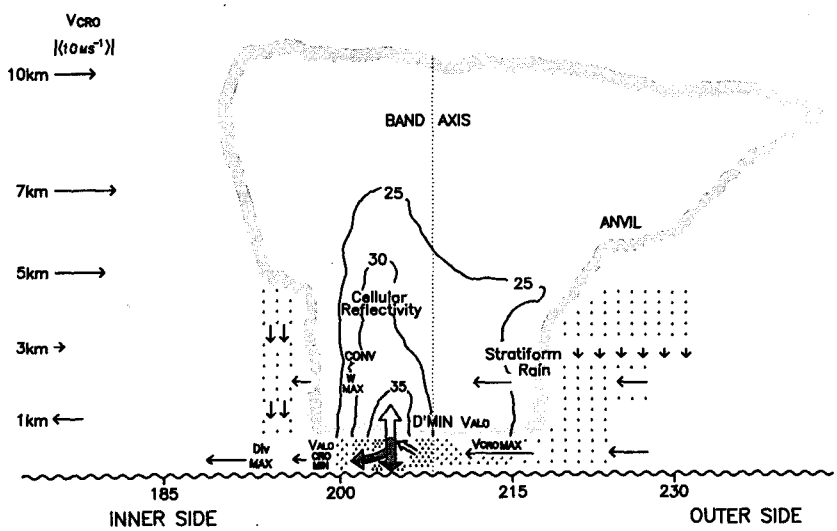

FIG. 16. Schematic model of rainband precipitation and kinematic structure. (a) Plan view, showing positions of relative maxima and minima of reflectivity and kinematic fields based on crossband flight legs. Inner side of the rainband is to the left. (b) Rainband in crossband-height cross section. Outer solid line indicates cloud edges, contours represent radar reflectivity, horizontal arrows show crossband component of the flow, bold vertical arrows indicate convective core updrafts and downdrafts.

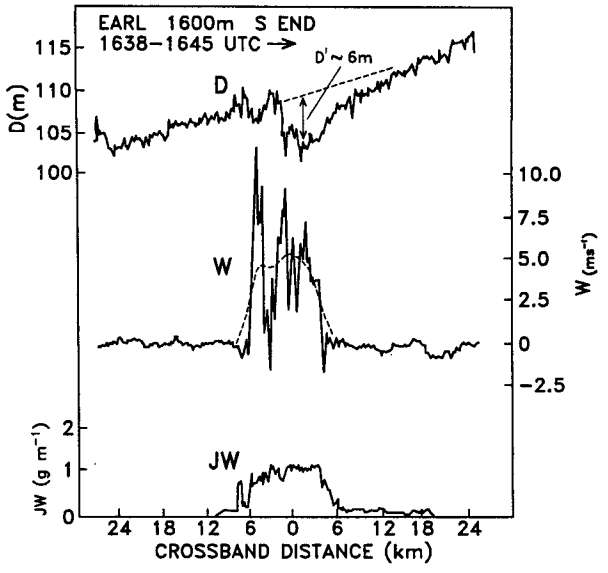

FIG. 17. Crossband profiles of 1 s values of D-value, vertical velocity, and JW cloud liquid water content for a west-to-east transect across the southern end of the Earl rainband from 1638 to 1644 UTC at 1600 m altitude. Deviation of D-value from dashed line is an estimate of the D-value perturbation.

southern end of the Earl rainband. It should be noted that the strongest 10% of hurricane updrafts (Jorgensen et al. 1985) at the 1500 m level have peak velocities of 4.6 m s^{-1}, and diameters of 3 km. Of the 6 passes at 1500 m in Earl and Josephine, 5 sampled updraft cores with peak velocities of over 8 m s^{-1} and diameters of 2–4 km. Therefore, the sample collected in Josephine and Earl appears to be stronger than that gathered by Jorgensen et al. 1985. In this section, we speculate on causes of the pressure perturbation field and its effect on the horizontal flow field.

The mesoscale studies of the GATE rainband of 14 September 1974 by LeMone (1983) and Zipser et al. (1981) are perhaps the most complete set of aircraft observations of a tropical rainband. This band was slow-moving (2.5 m s^{-1}) and aligned along the low-level wind (and shear) direction. A trailing stratiform anvil extended along the upper level shear vector. The similarity of the GATE band with many of the features of Fig. 16 leads to application of their results toward a qualitative explanation of the observed pressure perturbation and wind field.

a. Hydrostatic forcing of the pressure field

One possible explanation of the observed D' minimum is that it is produced hydrostatically. LeMone showed through a cloud model and convective-core statistics, that the GATE rainband pressure minimum was produced hydrostatically by warm, moist air in the mesoscale updraft region of the band. In the rainband HPBL experiments discussed here, we did not obtain the middle and upper level convective-draft statistics and virtual temperature observations needed to calculate the hydrostatic effect. Considering the higher equivalent potential temperatures usually observed in hurricane convective updrafts (e.g., Powell 1990; Marks 1985), it is possible that a portion of the mesoscale pressure minimum observed across the band is hydrostatic. It should be noted that both BZJM and LeMone found evidence of a weak mesoscale high-pressure region at the 150 m level, almost directly below the rainband mesolow, produced by cold saturated downdraft air with high liquid water content. Evidence of such a mesohigh was noted in the 150 and 260 m level transits of the northern section of the Earl band that was associated with a downdraft (Fig. 13e). No such evidence was found in Irene (Barnes and Stossmeister 1986), and no 150 m level legs were flown across the Josephine rainband.

b. Dynamic forcing of the pressure field

On the convective scale, nonhydrostatic or dynamic forces of the type discussed by Rotunno and Klemp (1982) should be considered as a cause for pressure perturbations in rainbands. Since the analyses of the Josephine and Earl rainbands contain convective-scale influences as well as mesoscale two-dimensional fields, an alternate cause of the D' minimum may involve dynamic forcing on the updrafts of convective elements that make up the band.

According to Rotunno and Klemp, a perturbation pressure minimum is related to the interaction of an updraft with the vertical shear of the horizontal wind by

$$p' \propto (D\mathbf{V}/DZ)\cdot\nabla\mathbf{W}', \qquad (5)$$

where $(D\mathbf{V}/DZ)$ is the wind shear vector and $\nabla\mathbf{W}'$ is the horizontal gradient of the vertical velocity perturbation. This effect produces a perturbation pressure maximum on the upshear side of the updraft and a minimum on the downshear side. If the wind shear vector veers with height, the vertical orientation of the perturbation pressure may allow the updraft to be enhanced on one side and inhibited on another.

In a hurricane rainband, with a shear vector and crossband kinematic structure similar to that of Earl, the schematic in Fig. 18 illustrates the geometry of possible dynamic forcing. In plan view, the wind shear effect produces a pressure minimum on the outer side of the updraft. Since the updraft in Fig. 16b is on the inner side of the rainband axis, this effect should occur near the band axis, where the pressure minimum is indeed observed. Hence, this mechanism is likely because it explains the phase separation of the D' minimum and the updraft axis. LeMone et al. (1987) also found such a phase difference in the Cooperative Convective Precipitation Experiment (CCOPE) perturbation pressure fields near cloud-base updrafts. Their calculations of the perturbation pressure field produced

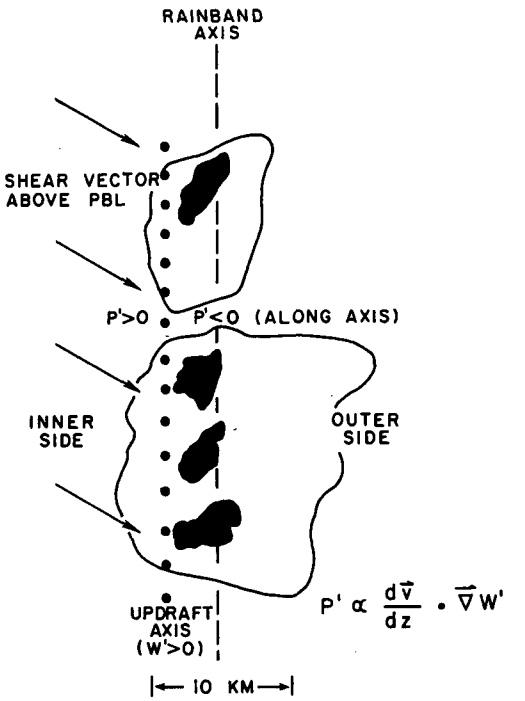

FIG. 18. Schematic diagram of the interaction of the vertical shear of the horizontal wind (arrows from left to right) with the rainband-scale updraft axis (filled circles), resulting in a perturbation pressure minimum near the reflectivity axis (reflectivity maxima indicated by filled irregular shapes).

by the interaction of the updraft with the environmental wind shear gave good agreement with observations. A similar calculation using Eq. (6) of LeMone et al. (1987) and parameters derived from the profile shown in Fig. 17 (wavelength of 12 km, maximum filtered vertical velocity of 5 m s^{-1}, shear of 3.3×10^{-3}) gave a pressure perturbation of 0.63 mb, about the same as the observed value of 0.6 mb.

Rotunno and Klemp (1982) also suggest that if the wind veers with height from the surface upward, the vertical pressure gradient should enhance updrafts on the upband or upwind side of an individual convective cell (p' positive in the PBL and negative at upper levels) and inhibit updrafts on the downband or downwind side of a cell. Hence, cells on the upwind side of a precipitation element may be developing while cells on the downband side of the element are mature or decaying. It is difficult to ascertain from the radar data whether this shift was actually occurring, but development of cells on the upwind or upband ends of rainbands has been observed in land-based radar studies (e.g., Parrish et al. 1983).

c. *Pressure acceleration effects on the crossband wind field*

LeMone (1983) found that the observed mesoscale two-dimensional flow field in the GATE rainband could be explained in terms of an air parcel's response to a pressure gradient. In the boundary layer of the Josephine and Earl rainbands, the crossband variation of V_{cro} is partially explained by the band scale pressure gradient associated with the D value perturbation minimum located at or near the band axis in the majority of passes. In a two-dimensional sense, as air parcels approach the band axis from the outer side of the HPBL, they are accelerated through and around heavy rain (occasionally mixing with convective downdrafts that may reach the surface) by the pressure field on the outer side of the axis where the maximum crossband component is found. The mean D value perturbation gradient [from the filtered D values of all (6) Josephine and Earl 1500 m level passes] was 2 m over 10 km. This gradient is sufficient to produce a crossband acceleration of 2 m s^{-1}/km which is on the order of the observed accelerations (0.5–1 m s^{-1}/km). West of the axis, air parcels are decelerated by the perturbation pressure field, causing a minimum crossband wind component. Here, maximum low-level convergence helps to force the band-scale updraft.

If the band is moving outward relative to the storm, as in the Earl case before 1830 UTC, the band-relative crossband flow is enhanced and flow from the outer side will continue across the band after a portion rises and mixes in the convective ascent region. If the band is stationary relative to the storm, as in the Josephine case, the crossband flow from the outer side may decelerate to zero on the inner side of the axis, where it is met by air approaching the ascent region from the inner side (being accelerated by the pressure field). In this case, the updraft region may behave as a total barrier to crossband flow that is approaching from both sides of the rainband, forcing the air to rise and mix with adjacent convective downdraft air, or causing the air to flow around the most intense cells.

d. *Vorticity generation effects on the alongband wind field*

The crossband variation of the alongband component of the flow in the GATE rainband was explained by Zipser et al. (1981) in terms of vorticity generation in air approaching the mesoscale updraft region. Rotunno and Klemp (1982) suggest that the tipping term of the vorticity equation,

$$D\zeta/Dt = \mathbf{k} \cdot (D\mathbf{V}/DZ \times \nabla \mathbf{W}'), \qquad (6)$$

can create a perturbation in the vertical component of vorticity. If we assume that most of the vertical shear of the horizontal wind in the HPBL occurs in the sur-

face and subcloud layers, then the orientation of the shear vector in the lower 700 m is directed mainly along the band. This is supported by the Earl hodograph in Fig. 7b and shown in the schematic in Fig. 16a. As such, horizontal vortex tubes would cross the band as depicted in Fig. 19. For Earl, the upward tipping of horizontal vortex tubes in the HPBL would generate positive relative vorticity on the outer side of the updraft, near the band axis. This term would combine with the stretching or spinup effect produced by the collocation of maximum low-level convergence and the updraft on the inner side of the axis to form a broad region of positive vorticity generation. For Josephine, with smaller alongband-directed, low-level shear, the effect would be limited to the lower 500 m. Therefore, within the HPBL, as inflowing air parcels approach from the outer side, this region of vorticity generation may be evident as a cyclonic shear zone (stronger V_{alo} on the outer side of the axis and weaker V_{alo} on the inner side). The upward transport of low V_{alo} air from the HPBL in the updraft region also contributes to the V_{alo} minimum on the inner side of the band axis.

7. Summary and comparison to tropical squall lines

a. Summary

The mesoscale rainfall and kinematic structures of Hurricanes Josephine and Earl show many characteristics that appear to be typical of well-organized, convective outer rainbands:

1) The rainbands were 15–20 km wide, as defined by the 25 dBZ contours of TA radar VI cross sections. They comprised a linear aggregate of precipitation elements containing individual cellular reflectivity maxima that were constantly developing, maturing and decaying over time scales of 15–30 min. The band axes were oriented perpendicular to the vertical shear vector of the low-level (0.5–6 km) horizontal wind. The cells were located preferentially toward the upshear side of the band axis and moved along the band at speeds of about 85% of the 0.2–6 km density-weighted mean wind. Cellular reflectivity was oriented vertically or with an outward tilt, with towers up to 7–9 km altitude and stratiform reflectivity extending outward as far as 20 km from the axis.

2) Crossband profiles from 150–1650 m in both storms indicate that the inner side of the rainband axis is the preferred region for convective-scale vertical drafts with 60% updrafts and 40% downdrafts, as found by BZJM in Hurricane Floyd (1981). The mesoscale fields across the band also show an updraft axis on the inner side of the axis and a D-value perturbation minimum at the axis. The band-relative wind field exhibits a strong cyclonic horizontal shear across the band, with along- and crossband wind maxima on the outer side of the band and corresponding minima on the inner side. Maximum convergence is near the updraft axis, with maximum vorticity between the updraft and rainband axes. Divergence regions are occasionally noted that extend 20 km to either side of the band in subsidence areas.

3) The location of the D' minimum with respect to the updraft axis is similar to that found by LeMone and co-workers in a slow-moving GATE rainband and in midlatitude convection. The relative positions can be qualitatively explained using the arguments of Rotunno and Klemp (1982) as an interaction of the wind shear with the vertical velocity gradient at the updraft axis. The crossband pressure gradient force implied by the D' gradient helps to explain the outer V_{cro} maximum. Relative vorticity in the HPBL is produced near the band axis where crossband-directed horizontal vortex tubes are tipped upward. This is evident as an increase in cyclonic shear across the band, with minimum V_{alo} on the inner side and maximum V_{alo} on the outer side of the band.

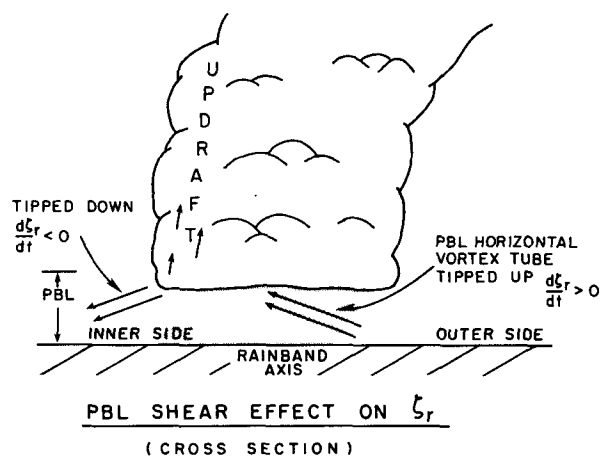

FIG. 19. Schematic diagram of the generation of vertical relative vorticity through tipping of shear-produced horizontal vortex tubes (double arrows) in the boundary layer. The boundary layer shear ve directed into the page, down the rainband.

b. Comparison with tropical squall lines

The hurricane rainbands discussed here have many of the characteristics of tropical rainbands and squall lines, both within and above the boundary layer (e.g., Betts et al. 1976; Houze 1977; Zipser 1969, 1977; Gamache and Houze 1982; Barnes and Sieckman 1984; Chong et al. 1987). Similarities include:

1) Orientation of the convection is perpendicular to the low-level crossband or crossline vertical shear vector of the horizontal wind.

2) Stratiform rain regions extend mostly downshear above 4 km. However, both can have anvils that overhang upshear as well.

3) Maximum low-level convergence and barrier effects are at the mesoscale updraft position with pressure minima produced by hydrostatic and dynamic effects.

4) Warm, moist, low-level inflow can be supplied from the relatively undisturbed environment ahead of the system's direction of motion, the more disturbed environment on the inner side of the band (Ishihara 1986), or from both sides of the band [e.g., Josephine (Figs. 9d, 10d) and both front to rear and rear to front inflow in the tropical squall line observed by Chong et al. 1987].

5) Surface cold pools contain θ_E decreases (Powell 1990) of 10–20 K from surrounding environmental values and help to force the mesoscale updraft.

Major differences involve structure of the leading and trailing edges and the speed and manner of propagation:

1) The hurricane rainband updraft is on the upshear side of the band. The more intense cells are on the inner side of the band axis and contain cool convective-scale downdrafts. These cells move down the band at about 85% of the lower tropospheric mean wind. The downdrafts spread at the surface, but are too weak to propagate into the strong low-level inflow. Instead, they help to force the updraft and tend to spread in a shallow flow downwind on the inner side of the band. This cool dry air, subsidence on the inner side beneath the anvil, and the downshear extension of stratiform rain toward the outer side give the inner side of the band a "hard" reflectivity edge. This reflectivity structure and the relative locations of the updraft and stratiform rain give the inner trailing edge of the hurricane rainband the appearance of a squall-line leading edge.

2) As shown in Barnes and Sieckman (1984), GATE tropical squall lines form in an environment in which easterlies increase with height from 0–4 km. The downdrafts transport extremely low θ_E air down to the surface. The air spreads out at the surface as a gust front, moving westward at high speeds of 10–20 m s^{-1}. This motion causes a squall-relative flow from front to back at all levels, with maximum storm relative inflow near the surface. The line propagates by discrete growth of new cells which form at the front and move rearward relative to the system.

3) The hurricane rainband may be storm-stationary (e.g., Josephine, Earl after 1830 UTC, Floyd), outward-moving (e.g., Earl before 1830 UTC, examples from Senn and Hiser 1959) or intrinsically inward-moving (relative to the mean flow) while appearing to move outward (relative to the storm), (e.g., Caroline (1975) as described by Willoughby 1978). The outward motion of the Earl rainband before 1830 UTC is probably unrelated to the presence of a cold pool, because this feature was also observed (in a more extreme state) at 1930 UTC (Powell 1989) when the band was storm-stationary.

The outer convective rainband has a profound effect on the kinematic structure of the HPBL. The thermodynamic structure of the HPBL is also influenced greatly by rainband convection and has many similarities to those found in tropical rainband and squall-line studies. Thermodynamic changes produced by convective-scale downdrafts have the potential to modify large enough sections of the HPBL to have a negative feedback effect on surrounding convection and possibly even the eyewall. The companion paper, Powell (1990), examines the mesoscale thermodynamic features of the Josephine and Earl rainbands, the processes acting to maintain and renew mixed-layer structure, and the effect of HPBL modification on adjacent convection.

Acknowledgments. The author thanks Peter Black for his helpful discussions and Stanley Rosenthal for his support throughout all stages of the research. Robert Burpee provided many valuable suggestions, especially in the planning and early research phases of the study. The author benefited from discussions with many individuals including Frank Marks, John Gamache, Paul Willis, James Franklin and Hugh Willoughby of HRD and Rit Carbone of NCAR. Comments on earlier versions of the manuscript by Gary Barnes and an anonymous reviewer helped to improve the paper. The conscientious efforts of the NOAA Office of Aircraft Operations personnel and lead project scientists Peter Black and Frank Marks in executing the experiments is greatly appreciated. Neal Dorst and Joyce Berkeley assisted in programming and data reduction. David Senn, Joni David and Chris Labbé produced the graphics. Connie Arnhols contributed editorially and Andy Ramsay provided photography services.

REFERENCES

Anthes, R. A., 1982: Tropical cyclones: Their evolution, structure and effects. *Meteor. Monogr.*, **19**(41), Amer. Meteor. Soc., 208 pp.

Atlas, D., K. R. Hardy, R. Wexler and R. J. Boucher, 1963: On the origin of hurricane spiral bands. *Geofis. Int.*, **3**, 123–132.

Barnes, G. M., E. J. Zipser, D. P. Jorgensen and F. D. Marks, Jr., 1983: Mesoscale and convective structure of a hurricane rainband. *J. Atmos. Sci.*, **40**, 2125–2137.

——, and K. Sieckman, 1984: The environment of fast- and slow-moving tropical mesoscale convective cloud lines. *Mon. Wea. Rev.*, **112**, 1782–1794.

——, and G. J. Stossmeister, 1986: The structure and decay of a rainband in Hurricane Irene (1981). *Mon. Wea. Rev.*, **114**, 2590–2601.

Betts, A. K., R. W. Grover and M. W. Moncrieff, 1976: Structure and motion of tropical squall lines over Venezuela. *Quart. J. Roy. Meteor. Soc.*, **102**, 395–404.

Black, P. G., R. L. Elsberry, L. K. Shay, R. P. Partidge and J. F. Hawkins, 1988: Atmospheric boundary layer and oceanic mixed-layer observations in Hurricane Josephine obtained from air-deployed drifting buoys and research aircraft. *J. Oceanic. Atmos. Technol.*, **5**, 683–698.

Chong, M., P. Amayenc, G. Scialom and J. Testud, 1987: A tropical squall line observed during the COPT 81 experiment in West

Africa. Part I: Kinematic structure inferred from dual-Doppler radar data. *Mon. Wea. Rev.*, **115**, 670–694.
Gamache, J. F., and R. A. Houze, Jr., 1982: Mesoscale air motions associated with a tropical squall lines. *Mon. Wea. Rev.*, **110**, 118–135.
Gentry, R. C., 1964: A study of hurricane rainbands. NHRP Rept. No. 69, NOAA/AOML, 4301 Rickenbacker Cswy., Miami, FL 33149, 82 p.
Houze, R. A., Jr., 1977: Structure and dynamics of a tropical squall-line system during GATE. *Mon. Wea. Rev.*, **105**, 1540–1567.
Holland, G. J., 1982: Tropical cyclone motion: Environmental interaction plus a beta effect. *J. Atmos. Sci.*, **40**, 328–342.
Ishihara, M., Z. Yanagisawa, H. Sakakibara, K. Matsuura and J. Aoyagi, 1986: Structure of a typhoon rainband observed by two Doppler radars. *J. Meteor. Soc. Japan*, **64**, 923–939.
Jorgensen, D. P., 1984a: Mesoscale and convective-scale characteristics of mature hurricanes. Part I: General observations by research aircraft. *J. Atmos. Sci.*, **41**, 1268–1285.
——, 1984b: Mesoscale and convective scale characteristics of mature hurricanes. II: Inner core structure of Hurricane Allen (1980). *J. Atmos. Sci.*, **41**, 1287–1311.
——, P. H. Hildebrand and C. L. Frush, 1983: Feasibility test of an airborne pulse-Doppler meteorological radar. *J. Atmos. Sci.*, **22**, 744–757.
——, E. J. Zipser and M. A. LeMone, 1985: Vertical motions in intense hurricanes. *J. Atmos. Sci.*, **42**, 839–856.
Kurihara, Y., and R. E. Tuleya, 1974: Structure of a tropical cyclone developed in a three-dimensional numerical simulation model. *J. Atmos. Sci.*, **31**, 893–919.
LeMone, M. A., 1983: Momentum transport by a line of cumulonimbus. *J. Atmos. Sci.*, **40**, 1815–1834.
——, G. M. Barnes, J. C. Fankhauser and L. F. Tarleton, 1987: Perturbation pressure fields measured by aircraft around the cloud-base updraft of deep convective clouds. *Mon. Wea. Rev.*, **116**, 313–327.
Ligda, M. G., 1955: Hurricane Squall Lines. *Bull. Amer. Meteor. Soc.*, **36**, 340–342.
Marks, F. D., Jr., 1985: Evolution and structure of precipitation in Hurricane Allen (1980). *Mon. Wea. Rev.*, **113**, 909–930.
——, and R. A. Houze, Jr., 1984: Airborne Doppler radar observations in Hurricane Debby. *Bull. Amer. Meteor. Soc.*, **65**, 569–582.
Merceret, F. J., 1983: A study of NOAA WP-3D terminal navigation errors based on navigator's logbooks: 1977–83. NOAA Tech. Memo., OAO 2, NOAA/AOML, 4301 Rickenbacker Cswy., Miami, FL 33149, 63 p.
——, and H. W. Davis, 1981: The determination of navigational and meteorological variables measured by NOAA/RFC WP3D aircraft. NOAA Tech. Memo., ERL RFC-7, NOAA/AOML, 4301 Rickenbacker Cswy., Miami, FL 33149, 21 p.
Moss, M. S., 1978: Low-level turbulence structure in the vicinity of a hurricane. *Mon. Wea. Rev.*, **106**, 841–849.
——, and F. J. Merceret, 1976: A note on several low-level features of Hurricane Eloise (1975). *Mon. Wea. Rev.*, **104**, 967–971.
Ooyama, K. V., 1982: Conceptual evolution of the theory and modeling of the tropical cyclone. *J. Meteor. Soc. Japan*, **60**, 369–380.
Parrish, J. R., R. W. Burpee, F. D. Marks, Jr. and C. L. Landsea, 1984: Mesoscale and convective-scale characteristics of Hurricane Frederic during landfall. *Postprints, 15th Conf. on Hurricanes and Tropical Meteorology*, Miami, FL, Amer. Meteor. Soc., Boston, 415–420.
Powell, N. D., 1987: Changes in the low-level kinematic and thermodynamic structure of Hurricane Alicia (1983) at landfall. *Mon. Wea. Rev.*, **115**, 75–99.
——, 1988: Boundary layer structure and dynamics in outer hurricane rainbands. PhD. dissertation, The Florida State University, 227 pp., #8822464, UMI 300 N. Zeeb Rd., Ann Arbor, MI 48106.
——, 1990: Boundary layer structure and dynamics in outer hurricane rainbands, Part II: Downdraft modification and mixed-layer recovery. *Mon Wea. Rev.*, **118**, 918–938.
——, and P. G. Black, 1984: Airborne Doppler radar observations of the boundary layer of Hurricane Debby (1982). *Preprints, 22nd Conf. on Radar Meteorology*, Zurich, Switz., Amer. Meteor. Soc., Boston, 584–588.
Rotunno, R., and J. B. Klemp, 1982: The influence of the shear-induced pressure gradient on thunderstorm motion. *Mon. Wea. Rev.*, **110**, 136–151.
——, J. B. Klemp and M. L. Weisman, 1988: A theory for strong, long-lived squall lines. *J. Atmos. Sci.*, **45**, 463–485.
Senn, H. V., and H. W. Hiser, 1959: On the origin of hurricane spiral bands. *J. Meteor.*, **16**, 419–426.
Shapiro, L. J., 1983: The asymmetric boundary layer flow under a translating hurricane. *J. Atmos. Sci.*, **40**, 1984–1998.
Simpson, R. H., and L. G. Starrett, 1955: Further studies of hurricane structure by aircraft reconnaissance. *Bull. Amer. Meteor. Soc.*, **36**, 459–470.
Staff Members, Tokyo University, 1969: Precipitation bands of Typhoon Vera in 1959 (Part I). *J. Meteor. Soc. Japan*, **47**, 298–309.
Tatehira, R., 1961: A mesosynoptic and radar analysis of typhoon rain band, case study of typhoon "Helen," 1958. *Proc. 2nd Tech. Conf. on Hurricanes*, Miami, Amer. Meteor. Soc., 115–126.
Ushijima, T., 1958: Outer rainbands of typhoons *J. Meteor. Soc. Japan*, **36**, 1–10.
Weisman, M. L., and J. B. Klemp, 1982: The dependence of numerically simulated convective storms on vertical wind shear and buoyancy. *Mon. Wea. Rev.*, **110**, 504–520.
Wexler, H., 1947: Structure of hurricanes as determined by radar. *Ann. N.Y. Acad. Sci.*, **48**, 821–844.
Willoughby, H. E., 1978: A possible mechanism for the formation of hurricane rainbands. *J. Atmos. Sci.*, **35**, 838–848.
——, J. A. Clos and M. G. Shoreibah, 1982: Concentric eyewalls, secondary wind maxima, and the evolution of the hurricane vortex. *J. Atmos. Sci.*, **39**, 395–411.
——, F. D. Marks, Jr. and R. J. Feinberg, 1984: Stationary and propagating convective bands in asymmetric hurricanes. *J. Atmos. Sci.*, **41**, 3189–3211.
Zipser, E. J., 1969: The role of organized unsaturated convective downdrafts in the structure and rapid decay of equatorial disturbance. *J. Appl. Meteor.*, **8**, 799–814.
——, 1977: Mesoscale and convective-scale downdrafts as distinct components of squall-line circulatin. *Mon. Wea. Rev.*, **105**, 1568–1589.
——, R. J. Meitin, and M. A. LeMone, 1981: Mesoscale motion fields associated with a slowly moving GATE convective band. *J. Atmos. Sci.*, **38**, 1725–1750.